Laser and Particle Beams, page 1 of 7, 2016.

doi:10.1017/S0263034616000069

Temporal distribution of the electrical energy on an exploding wire

GONZALO RODRÍGUEZ PRIETO,[1] LUIS BILBAO,[2] AND MALENA MILANESE[3]

[1]Universidad de Castilla-La Mancha, E.T.S.I.I. Ciudad Real, Spain
[2]Instituto de Física del Plasma, UBA-CONICET Buenos Aires, Argentina
[3]CONICET, Universidad Nacional del Centro de la Provincia de Buenos Aires Instituto de Física Arroyo Seco - Facultad de Ciencias Exactas, Tandil, Argentina

(Received 21 December 2015; Accepted 18 January 2016)

Abstract

An exploding wire system has been experimentally studied by the observation of its plasma dynamics and the electrical energy delivered by the supporting circuit to the metallic wire. Plasma radial expansion has been obtained from visible light streak images, meanwhile electrical energy transfer dynamics was derived from the analysis of voltage and current traces of the exploding wire circuit. In these measurements, a significant portion of the electrical energy has been transferred to the exploding wire circuit during the plasma expansion, and lower limits for the resistivity during the plasma expansion confirm the existence of a central liquid or solid metallic core in addition to the expanding plasma.

Keywords: Exploding wire; Radial dynamics; Resistivity

1. INTRODUCTION

Exploding wire systems have a long history in modern science, starting from the observation of a metallic wire length shortening after intense electrical currents through the wire at the end of the nineteenth century (Nairne, 1780) until more actual works, such as the use of exploding wires as explosive initiators (Liverts *et al.*, 2015). Some of the most unusual applications of an exploding wire system are controlled generation of large volumes of linear plasma (Smith *et al.*, 2007), or the use of a wire as coil for a high voltage transformer (Sinton *et al.*, 2009). One of the most promising technological applications of the exploding wire system is the generation of metallic nanopowders (Kotov, 2003), were some works dealing with Aluminum (Al) nanopowders show a dependence on the particle size with the deposited energy (Sindhu *et al.*, 2008).

On the other hand, with small groups of wires it is possible to reach very high pressures when the wires are properly arranged and surrounded by a dense medium such as water (Efimov *et al.*, 2008; Krasik *et al.*, 2006, 2008), and these pressures had been experimentally proven enhanced by the presence of a metallic pressure reflector close to the wire arrangement (Gilburd *et al.*, 2012). Exploding wires are the capital in the Sandia Z facility, because of the arrangement of hundreds of tungsten (W) wires in a circular shape to create a cylindrically imploding plasma which leads to one of the most intense artificial X-ray generators known today (Sinars *et al.*, 2006). Such complicated systems are challenging to simulate and understand properly, the coupling between the electrical circuit delivering the energy and the plasma formation and evolution in the wire systems as one of the difficult problems (Jennings *et al.*, 2010). Challenge is worth due to the insight in very special states of matter obtained in facilities with access to these devices, as the first experimental probing of the dense liquid deuterium insular-to-metal transition in the Sandia laboratory demonstrates (Knudson *et al.*, 2015). With different scales on the range of possible energies delivered to the wire, exploding wires systems has been used to probe metallic properties near the boiling point (Chandler *et al.*, 2002), explore the equation of state, and conductivity of non-ideal plasmas (Sheftman & Krasik, 2010; Stephens & Neuber, 2012), and the generation of metallic elements X-ray spectra (Burkhalter *et al.*, 1977).

Exploding wire process, therefore, has been extensively researched in many areas, from which a picture of the temporal process of plasma conversion from a cold, solid core has emerged within the years. From this description, the electrical energy transferred to the wire appears as an important parameter, as plasma properties show a strong dependence from

Address correspondence and reprint requests to: Gonzalo Rodríguez Prieto, Universidad de Castilla-La Mancha, E.T.S.I.I. Ciudad Real, Spain. E-mail: gonzalo.rprieto@uclm.es

this magnitude (Vijayan & Rohatgi, 1985; Sarkisov *et al.*, 2005), while the surrounding medium influences the final energy deposition to the wire. Increase in medium density is followed by an increase in the deposited electrical energy on the wire thanks to the neutralization of voltage breakdown of the metallic vapor in denser media (Ter-Oganesyan *et al.*, 2005).

Exploding wire temporal evolution starts with the initial Joule heating of the solid wire, followed by the generation of metallic vapor from the wire surface that became plasma due to the electrical field between the wire poles. Then the, current is transferred to the plasma (Duselis & Kusse, 2003), and the remaining solid core is transformed by the plasma wave traveling inwards, meanwhile electrical energy transfer is halted due to the low resistance of the plasma sheath surrounding the wire core.

This work is devoted to the experimental observation of electrical energy transference from the circuit to the wire solid or liquid core after plasma formation for copper (Cu), tungsten, and molybdenum (Mo) wires. It is distributed as follows: after this section, Section 2 deals with the experimental setup and data analysis, meanwhile in Section 3, results are presented, and in the last section some conclusions are presented.

2. EXPERIMENTAL SETUP

ALEX experimental construction is a typical exploding wire setup. The wire is surrounded by atmospheric air and has a fixed length of 3 cm. Two capacitors of ~1.1 μF each are connected in parallel with a high voltage source, which in these experiments delivered a maximum of 25 kV. Spark gap trigger separates this circuit section from the exploding wire supports, which finishes with the earth pole connection.

In order to diagnose both the electrical circuit and plasma formation, some probes had been attached to the main circuit, see Figure 1. A resistive divider as voltage probe and a Rogowski coil for current measurements were placed in direct contact with the wire holders, in order to observe the voltage and current values in the wire. The two sensors had been intentionally placed close to the wire holders, in order to prevent the interference of other parts of the circuit with the signals and to overcome the difficulties in the data interpretation, such as the significant current loses observed in (Jennings *et al.*, 2010). Both probes had been made and calibrated in the laboratory, with the intensity derived from the Rogowski coil signal by means of numerical integration. In addition, to allow the synchronization with other optical sensors, a fast photodiode signal (rise time ~1 ns) is synchronized and recorded with the electrical signals. Finally, a streak camera focused on the wire allows the recording of the plasma wire expansion using visible light plasma emissions.

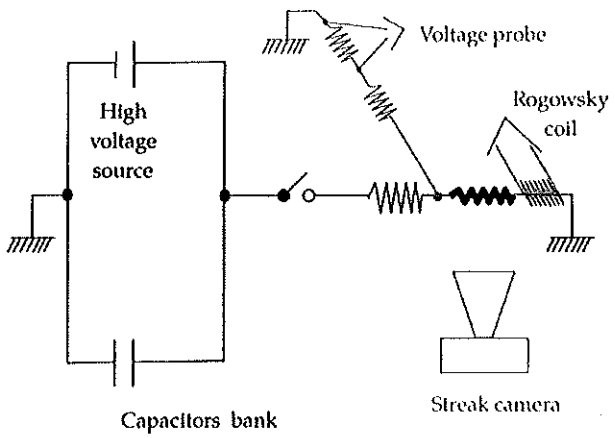

Fig. 1. ALEX electrical and probes scheme.

Digital streak camera photos are first scaled from pixel to space–time coordinates and then the radius is obtained using a simple Octave script that also approximates the radial expansion to the function $r = \sqrt{\beta \cdot t}$, a result obtained by considering the self-similar wire plasma expansion, as it has been proved to be a good approximation earlier (Bennett, 1969), despite problems with the validity of the self-similar hypothesis in such system (Bennett, 1961).

From this radial approximation and within the self-similar hypothesis for pressure, density, and velocity of the plasma expansion, the kinetic energy of the plasma expansion can be estimated using the formula:

$$E = \beta^2 \cdot \rho \cdot l_w, \tag{1}$$

where β is the previously defined constant, ρ is the air density as it is against this fluid that the expansion is made, and l_w, the wire length (Bennett, 1958).

On the other hand, more complicated calculations are to be made with the electrical signals as the voltage registered by the resistive divider is the addition of two terms, one the voltage that is dynamically consumed in the exploding wire process and other, voltage used by the static parts of the circuit. Therefore, it is necessary to remove this last term from the resistive divider signal.

To do so, the total inductance of the circuit is to be frequently used, as the wire inductance can be considered negligible. In the work presented here, a different method has been employed and the resulting signal has a clear reduction in the noise level, so it is worth to dedicate a few words to its description.

Let us consider the voltage and current signals recorded by the sensors, of which a typical example is presented in Figure 2. Then it is possible to realize that the last part of the voltage time evolution is dominated by a simple exponential decay, that can be calculated by $l \cdot \frac{\partial I}{\partial t} + r \cdot I$, with l and r as the constant inductance and resistance of the static circuit part, formed mainly by the wire holders and the space between them, meanwhile I is the current that passes through the metallic wire. As both the values of the current and its

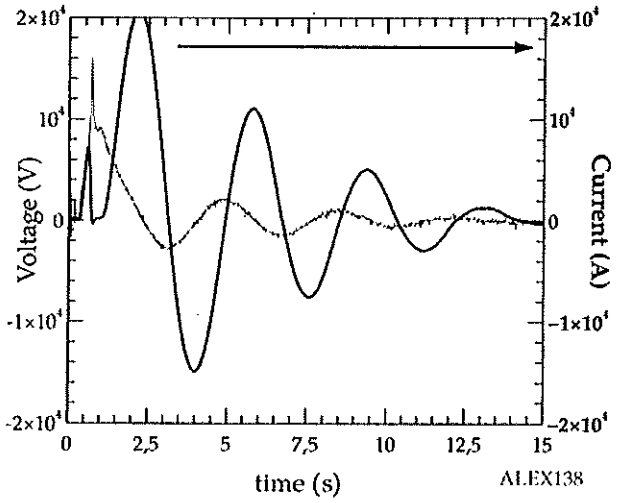

Fig. 2. Typical total voltage (points) and current (continuous) traces.

derivative are simultaneously measured, it is possible to adjust the values of l and r so as to make the measured final voltage signal coincide with the previous expression by means of a minimal square regression, and then subtract this voltage value from the total, in order to obtain the voltage circulating through the wire, as Figure 3 shows, is far from an oscillation, due to the highly dynamic nature of the exploding wire process. As was typical in our experiments, the so called dark current pause (Bibbo *et al.*, 1998) is clearly observed.

With these two magnitudes it is possible to obtain interesting derivate magnitudes, namely in this work, the power that circulates through the exploding wire, and its resistance and resistivity. Power can be easily calculated, as it is the integral of the product of the voltage and current magnitudes. Resistance and resistivity cannot be calculated directly, as some assumptions and approximations are needed for their deduction from the measured values of voltage and current.

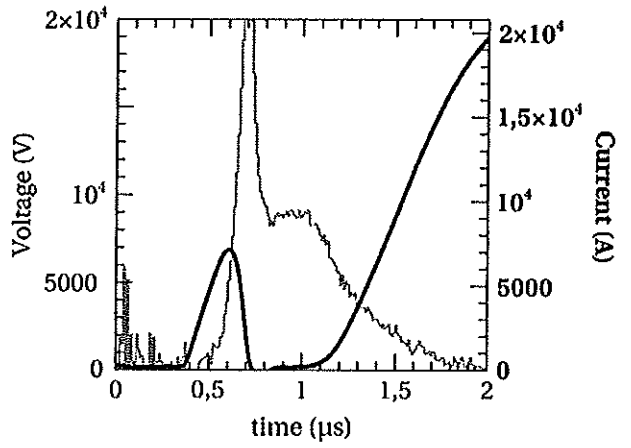

Fig. 3. Wire voltage (points) and current (continuous) signals. Notice the change in time scale.

Exploding wire systems possess an inductance that changes in time, therefore the wire voltage can be written as:

$$V = R \cdot I + L \cdot \dot{I} + \dot{L} \cdot I, \tag{2}$$

where L and R are the wire inductance and resistivity, respectively. Resistance can then be obtained as follows:

$$R = \frac{V}{I} - L \cdot \frac{\dot{I}}{I} - \dot{L}. \tag{3}$$

Consequently, taking the typical values into account for the relevant magnitudes, negligibility of the subtraction terms in the above equation is obvious after some trivial algebra. Therefore, resistance can be approximated from the value obtained by considering the wire as resistor only.

Estimation of resistivity is not so easy, as the concept itself is more complex. Note that the electric field is:

$$\mathbf{E} = -\nabla V - \frac{\partial \mathbf{A}}{\partial t}, \tag{4}$$

where V is the scalar potential and $\mathbf{A}$ the vector potential. Then, the voltage difference along a given path is:

$$\Delta V_{AB} = -\int_A^B \left(\mathbf{E} + \frac{\partial \mathbf{A}}{\partial t}\right) \cdot \mathrm{d}\mathbf{l}. \tag{5}$$

Since the current diffuses from the boundary, it holds that during diffusion, on the axis

$$\frac{\partial \mathbf{A}}{\partial t} \ll \mathbf{E}. \tag{6}$$

Therefore, using a path along the axis of the wire, see Figure 4, and assuming that the axial coordinate (z) is an ignorable coordinate we get

$$\Delta V_{AB} = -(E_z)_{axis} l_w, \tag{7}$$

where l_w is the length of the wire. Further, using an Ohm's law for the wire (whereas is solid, liquid, gas, or plasma),

$$\mathbf{E} = \mu \mathbf{j}, \tag{8}$$

where μ is the resistivity and j is the current density, it is possible to obtain:

$$\Delta V_{AB} = -(\mu j_z)_{axis} l_w, \tag{9}$$

From the above equation a lower limit to the resistivity of the wire may be deduced. Assuming that during the rise of the current, when the current is diffusing towards the axis, the current density on the axis is lower than the mean value of the current density on the whole wire, that is $(j_z)_{axis}$

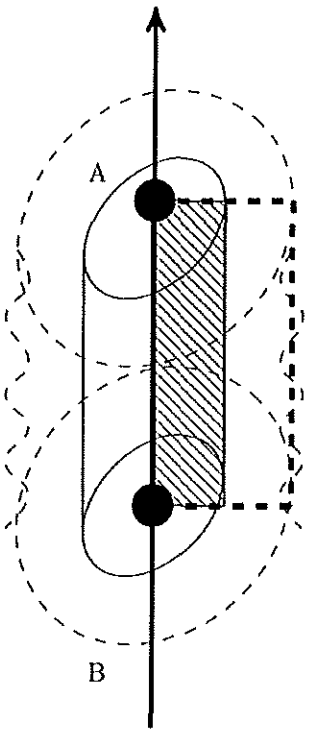

Fig. 4. Wire resistivity scheme. Continuous thick line, internal integration path; dashed thick line, external.

$<1/s_w>$, with s_w the section of the wire, therefore:

$$\mu_{axis} > \frac{\Delta V_{AB}}{I}\frac{s_w}{l_w}. \tag{10}$$

A legitimate question arose with the plasma presence, because then the electric field between the electrodes could be approximately zero, an apparent contradiction with the previous equation. But although at the border of the plasma it is possible to think that resistivity approaches zero, $\mu \approx 0$, using Eq. (5) the final result is:

$$\Delta V_{AB} = -\left(\frac{\partial A_z}{\partial t}\right)_{border} \cdot l_w. \tag{11}$$

Now, it is clear that the voltage across the boundary is almost due to the electromotive force (emf) caused by the electromagnetic induction (Faraday's law of induction). Note that the emf is due to both the movement of the boundary and simultaneous current diffusion through the wire, since both produce a variation of the magnetic flux enclosed by the border. Therefore, Faraday induced voltage is a missing parameter, following Figure 4 such voltage can be calculated as the integral of the electric field along the closed line that forms the hatched rectangle in the figure. So in the vertical lines, it is legitimate the assumption of electric field as negligible, but on the horizontal lines this is not the case as current density is distributed along the surface, forcing its

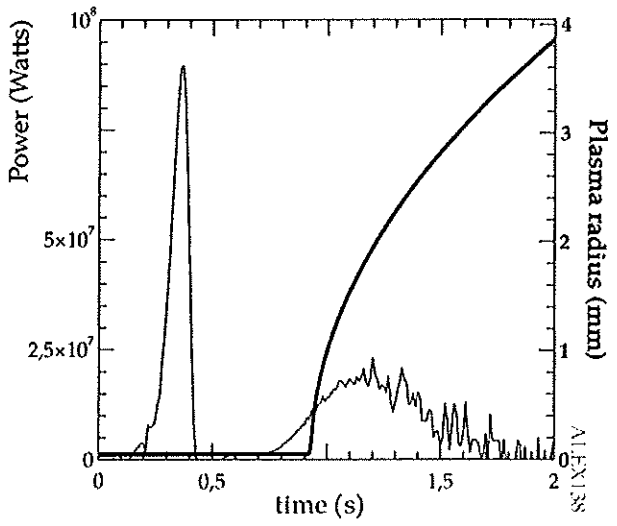

Fig. 5. Electrical power (thin line) and radius (thick line) on a typical experiment. Notice the presence of delivered power after the radial expansion of the plasma has started.

final value to be different from zero. Therefore, Faraday induced voltage and then the electric potential between the electrodes is nonzero despite the fact that there is an expanding plasma between them.

3. RESULTS AND DISCUSSION

Under the experimental conditions of the experimental series of this work, a significant amount of electrical energy is delivered to the wire after the beginning of the plasma expansion, as Figure 5 shows for a typical situation presented for a Cu wire of 100 μm of diameter when the capacitors were charged to 10 kV. Simultaneously, the low limit resistivity is too high to pertain to a plasma with values of an order of magnitude higher than the usual in a plasma, as measured by Esaulov *et al.*, 2011. Figure 6 shows the measured values of resistivity for the previous experiment. These two measurements clearly indicate that after plasma generation the wire system is still absorbing the electrical energy.

On the other hand, measurements of the kinetic energy with the method explained above, imply that the kinetic energy released to the wire must be done instantaneously, and without further energy additions to the moving material. This first condition, realistically means that the energy deposition rate is much faster than that of the following expansion, meanwhile the second one is to be applied to the portion of the wire that expands or moves; therefore, the fact that the measured kinetic energy is always smaller than the total electrical energy delivered to the wires, see Table 1, can be understood under the assumption that not all the wire mass take part on the self-similar kinetic release of energy observed in the streak images. Implicit in the data from the table is an absence of correlation between kinetic energy of the plasma and electrical energy delivered to the wire,

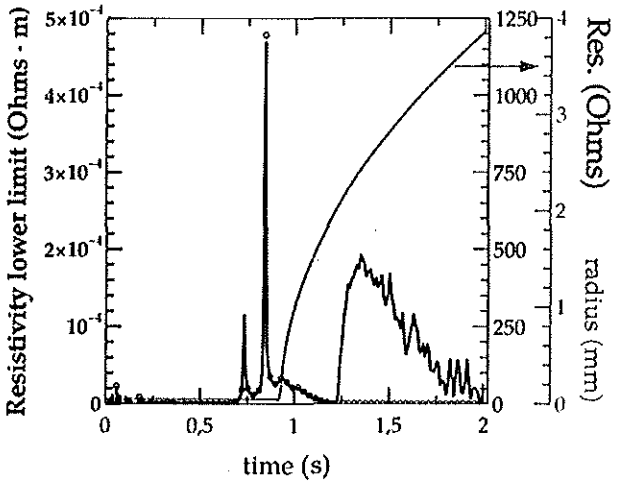

Fig. 6. Resistivity (continuous line), resistance (points), and radius (gray line). Visible is the initial resistivity peak as the wire is heated.

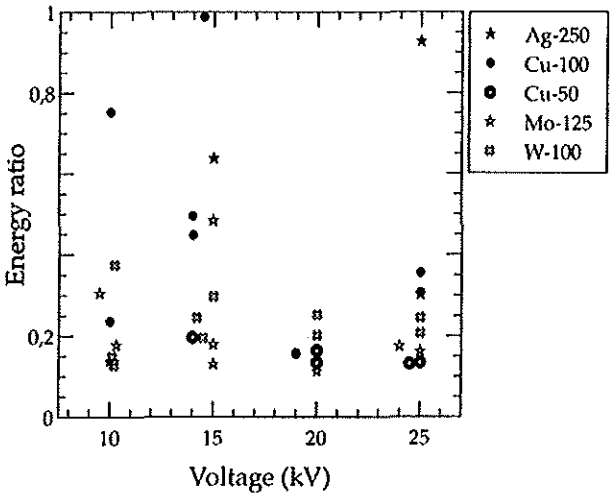

Fig. 7. Ratio of energies delivered in the first power peak to energy necessary to create and accelerate the plasma. Symbol legend indicates material and diameter in micrometers.

Table 1. *Metals and their energies ratios*

Metal (diameter in μm)	Charge voltage (kV)	Energies ratio
Cu (50)	14.0	0.20
Cu (50)	24.5	0.13
Cu (100)	10.0	0.24
Mo (125)	15.0	0.13
W (100)	14.5	0.20

Table 2. *Skin depth and diameters of the employed wires*

Metal	Cu	W	Mo	Ag
Approx. skin depth (μm)	61	39	105	60
Diameter (μm)	50–100	100	125	250

indicating that the relation between both energies depend on more parameters.

On the other hand, as Table 2 indicates, the skin depth of the employed metals is either shorter or on the same order of the wire's diameters. Under such conditions, the ablative model affirms that the wire should ablate fast and in a continuous manner, in contradiction with the previous statements about the wire ablation mass.

Indirect estimation of the wire fraction still on the core after the plasma generation is obtained from the ratio of two energies in this work. Namely, ratio of energy at the first power peak to the sum of the energy necessary to vaporize the wire with the self-similar kinetic energy and, as Figure 7 shows, this fraction is not very large, in coincidence with previous works (Sinars *et al.*, 2001; Chandler *et al.*, 2002). On the other hand, considering the ablation model outlined in the previous paragraphs, the fraction of energy absorbed by the wire should be larger for smaller diameters of the same material, because the ablated part of the wire is larger. However, the experimental results of this paper demonstrates the opposite behavior as the fraction of energy absorbed by Cu wire is significantly larger for the thicker diameters of 100 μm. In addition, although all the energy fractions are concentrated in a relatively small area, there is a clear tendency to be smaller as the larger the capacitors voltage gets, therefore as the initial energy increases the energy fraction decreases. Such behavior is not easy to understand within the frame of the ablation model, as an increase of the initial energy available to make the plasma should be followed by a larger amount of

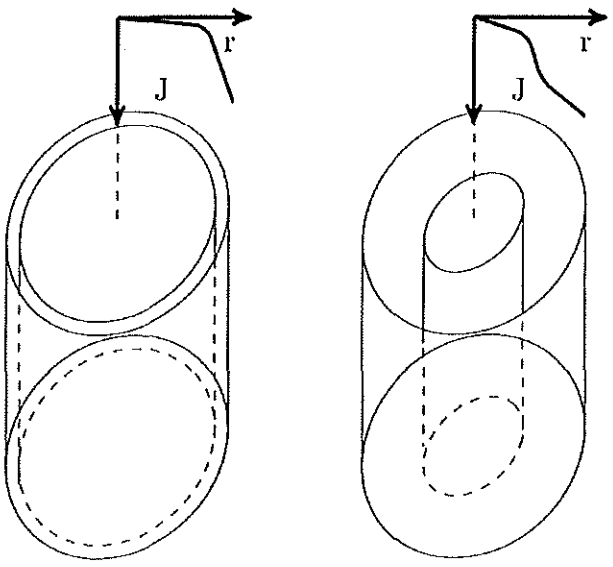

Fig. 8. Illustration of the two stages ablation process in a metallic wire, with the current density overimposed.

energy in the first power peak, and conversely a larger value of fraction energy presented in Figure 7.

In order to overcome these contradictions and from the experimental results shown here, we interpret them with a two stages ablation process. These processes start with the Joule heating of the wire surface because of the current circulating through it, frequently called the Ohmic phase. As the current value increases, the surface of the metallic wire becomes liquid and from there, it evaporates and creates a gas and finally a plasma region, meanwhile there is still a solid or liquid metallic wire core. With the calculated values for the skin depth shown on Table 2, current density on the wire system should be diffused through the entire the volume. Therefore, the current distribution will be mainly a function of the resistivity difference between the plasma and non-plasma parts of the wire system, effectively halting the current absorption of the non-plasma part due to its much higher resistivity. Our experimental data otherwise, indicates that there is a dynamical current diffusion time that is much larger than the one calculated for the stationary case. Such larger diffusion time allows for the inner solid core to maintain its current fraction for a longer period, therefore absorbing electrical energy despite of the external plasma presence. In our understanding, this means that there is a second plasma generation phase, fueled by the remaining electrical current flowing through the inner solid or liquid metallic core, see Figure 8.

4. CONCLUSIONS

In this paper, new experimental data on the exploding wire phenomena focused on the created plasma dynamics and its relation with the wire core behavior are presented. Such data first allow for the confirmation with diverse chemical elements and energies of previous observations on the auto-similarity of the radial temporal expansion of the plasma, extracted from its self-generated light, confirming data scattered across different previous works (Bennett, 1958, 1961; Chandler *et al.*, 2002). On the other hand, the combination of experiments on the exploding wire electrical circuit with plasma dynamic radial expansion obtained from streak data shows the existence of electrical energy transferred to the non-plasma part of the exploding wire, independent of its thermodynamical state.

ACKNOWLEDGEMENTS

The authors thank the fruitful discussions with A. R. Piriz and the technicians of the Engineering School of Ciudad Real and the INEI Institute, David Bocharán Murillo and Pedro Giménez de los Galanes García Muñoz for their help with the experimental facility. This work has been performed partially with financial support of the Spanish Ministerio de Economía y Competitividad project reference ENE2013-45661-C2-1-P and by the JCCLM of Spain (Grant No. PEII 11-0056-1890).

REFERENCES

Bennett, F.D. (1958). Cylindrical shock waves from exploding wires. *Phys. Fluids* **1**, 347–352.

Bennett, F.D. (1961). Shock waves from exploding wires at low ambient densities. Technical Report 1152, Ballistic Research Laboratories.

Bennett, F.D. (1969). High temperature exploding wires. *Progress in High Temperature Physics and Chemistry*, Vol. 2, pp. 1–61. London: Pergamon Press.

Bibbo, L., Giovambatista, N., Gomez, P., Olivieri, M., Tibaldi, C., Bernal, L., Pouzo, J. & Bilbao, L. (1998). Optical measurements in an exploding wire experiment. *Astrophys. Space Sci.* **256**, 467–472.

Burkhalter, P.G., Oozier, C.M. & Nagel, D.J. (1977). X-ray spectra from exploded-wire plasmas. *Phys. Rev. A* **15**, 700–717.

Chandler, K.M., Hammer, D.A., Sinars, D.B., Pikuz, S.A. & Shelkovenko, T.A. (2002). The relationship between exploding wire expansion rates and wire material properties near the boiling temperatue. *IEEE Trans. Plasma Sci.* **30**, 577–587.

Duselis, P.U. & Kusse, B.R. (2003). Experimental observation of plasma formation and current transfer in fine wire expansion experiments. *Phys. Plasmas* **10**, 565–568.

Efimov, S., Fedotov, A., Gleizer, S., Gurovich, V.Tz., Bazalitski, G. & Krasik, Ya.E. (2008). Characterization of converging shock waves generated by underwater electrical wire array explosion. *Phys. Plasmas* **15**, 112703.

Esaulov, A.A., Johnson, W.R., Safronova, A.S., Safronova, U.I., Kantsyrev, V.L., Weller, M.E. & Ouart, N.D. (2011). Plasma ionization and resistivity models in application to radiative properties of z-pinches. *High Energy Phys.* **8**, 217–223.

Gilburd, L., Efimov, S., Fedotov Gefen, A., Gurovich, V.Tz., Bazalitski, G., Antonov, O. & Krasik, Ya.E. (2012). Modified wire array underwater electrical explosion. *Laser Part. Beams* **30**, 215–224.

Jennings, C.A., Cuneo, M.E., Waisman, E.M., Sinars, D.B., Ampleford, D.J., Bennett, G.R., Stygar, W.A. & Chittenden, J.P. (2010). Simulations of the implosion and stagnation of compact wire arrays. *Phys. Plasmas* **17**, 092703.

Knudson, M.D., Desjarlais, M.P., Becker, A., Lemke, R.W., Cochrane, K.R., Savage, M.E., Bliss, D.E., Mattsson, T.R. & Redmer, R. (2015). Direct observation of an abrupt insulator-to-metal transition in dense liquid deuterium. *Science* **348**, 1455–1460.

Kotov, Yu.A. (2003). Electric explosion of wires as a method for preparation of nanopowders. *J. Nanopart. Res.* **5**, 539–550.

Krasik, Ya.E., Grinenko, A., Sayapin, A., Efimov, S., Fedotov, A., Gurovich, V.Z. & Oreshkin, V.I. (2008). Underwater electrical wire explosion and its applications. *IEEE Trans. Plasma Sci.* **36**, 423–434.

Krasik, Ya.E., Grinenko, A., Sayapin, A. & Gurovich, V.Tz. (2006). Generation of sub-Mbar pressure by converging shock waves produced by the underwater electrical explosion of a wire array. *Phys. Rev. E* **73**, 057301.

Liverts, M., Ram, O., Sadot, O., Apazidis, N. & Ben-Dor, G. (2015). Mitigation of exploding-wire-generated blast-waves by aqueous foam. *Phys. Fluids* **27**, 076103.

Nairne, E. (1780). An account of the effect of electricity in shortening wires. *Philos. Trans. R. Soc. London* **70**, 334–337. URL http://www.jstor.org/stable/106384

SINTON, R.P.W., HAMMOND, C., ENRIGHT, W. & BODGER, P. (2009). Generating high voltages with a plasma coil transformer. In *Proceedings of TechCon 2009*, 211–219.

SARKISOV, G.S., STRUVE, K.W. & MCDANIEL, D.H. (2005). Effect of deposited energy on the structure of an exploding tungsten wire core in a vacuum. *Phys. Plasmas* **12**, 052702.

SHEFTMAN, D. & KRASIK, YA.E. (2010). Investigation of electrical conductivity and equations of state of non-ideal plasma through underwater electrical wire explosion. *Phys. Plasmas* **17**, 112702.

SINARS, D.B., CUNEO, M.E., YU, E.P., LEBEDEV, S.V., COCHRANE, K.R., JONES, B., MACFARLANE, J.J., MEHLHORN, T.A., PORTER, J.L. & WENGER, D.F. (2006). Measurements and simulations of the ablation stage of wire arrays with different initial wire sizes. *Phys. Plasmas* **13**, 042704.

SINARS, D.B., HU, M., CHANDLER, K.M., SHELKOVENKO, T.A., PIKUZ, S.A., GREENLY, J.B., HAMMER, D.H. & KUSS, B.R. (2001). Experiments measuring the initial energy deposition, expansion rates and morphology of exploding wires with about 1 ka ~ Owire. *Phys. Plasmas* **8**, 216–230.

SINDHU, T.K., SARATHI, R. & CHAKRAVARTHY, S.R. (2008). Understanding nanoparticle formation by a wire explosion process through experimental and modelling studies. *Nanotechnology* **19**, 025703.

SMITH, D., ENRIGHT, W. & BODGER, P.S. (2007). A test circuit for long distance directional plasma discharge using the exploding wire technique. In *XVth International Symposium on High Voltage Engineering*, Ljubljana, Slovenia, pp. T3–489.

STEPHENS, J. & NEUBER, A. (2012). Exploding-wire experiments and theory for metal conductivity evaluation in the sub-eV regime. *Phys. Rev. E* **86**, 066409.

TER-OGANESYAN, A.E., TKACHENKO, S.I., ROMANOVA, V.M., MINGALEEV, A.R., SHELKOVENKO, T.A. & PIKUZ, S.A. (2005). Nanosecond electric explosion of a tungsten wire in different media. *Plasma Phys. Rep.* **31**, 916–926.

VIJAYAN, T. & ROHATGI, V.K. (1985). Characteristics of exploding-wire plasmas. *IEEE Trans. Plasma Sci.* **PS-13**, 197–201.

[2]

Laser and Particle Beams, page 1 of 7, 2016.

doi:10.1017/S0263034616000756

Exploding wire energy absorption dynamics at slow current rates

G. RODRÍGUEZ PRIETO,[1] L. BILBAO,[2] AND M. MILANESE[3]

[1]Universidad de Castilla-la Mancha, I.N.E.I., 13071, Ciudad Real, Spain
[2]Instituto de Física del Plasma, UBA-CONICET, 1428, Buenos Aires, Argentina
[3]CONICET, Universidad Nacional del Centro de la Provincia de Buenos Aires, Instituto de Física Arroyo Seco – Facultad de Ciencias Exactas 7000, Tandil, Argentina

(RECEIVED 13 September 2016; ACCEPTED 27 October 2016)

Abstract

Absorption of electrical energy provided to a metal wire in an exploding wire system is thought to be terminated or greatly diminished when the plasma is formed, after the joule heating of the metallic wire by the electrical current. Accordingly, it is common to account for the electrical energy delivered to the wire that the integration of current and voltage signals is halted when the voltage peak changes its slope. Usually, this moment is synchronized with the plasma appearance, as detected by optical sensors. In this work, experimental evidence of a two-step electrical energy absorption in an exploding wire surrounded by atmospheric air is presented. During the first step of the energy absorption the plasma is not formed, indicating that the delivered energy is not enough for ionizing the wire, giving place to a dark pause that lasts until a second energy absorption produces a plasma. The delay between the two steps can reach ≈2.2 μs for copper wires of 50 μm diameter charged at an initial voltage of 10 kV. Experimental investigation of variation of the delay between the two steps with different metals, charging voltages, and wire diameters are presented. A relation of the current density with the initial kinetic energy of the plasma and the electrical current rate is devised as a possible explanation of the observed phenomena.

Keywords: Exploding wires; Energy absorption dynamics; Dark pause

1. INTRODUCTION

When a high, fast electrical current flows through a metallic wire, the wire heats rapidly by the joule effect, changing its state from the solid to liquid, and then to gas to finally become a plasma. If the current is released in a controlled manner, then the exploding wire system is used as an experimental platform for plasma generation and many other associated research fields (Sarathi *et al.*, 2009; Sheftman & Krasik, 2010; Ram & Sadot, 2012; Stephens *et al.*, 2012). Despite of the fact that the experiment of a current passing through a conductor has been studied from the end of the 18th century (Nairne, 1780), it is after the middle of 20th century that the exploding wire phenomenon has been studied with more powerful measurement systems, as the review of Bennett *et al.* (1969) demonstrates. Along its history and until present times, scientific use of exploding wires covers a broad range of topics. Some examples are the experimental observation of metallic properties near boiling points of the metal (Chandler *et al.*, 2002), the generation of high-pressure shock waves on a dense medium, specifically in water (Sasaki *et al.*, 2006; Efimov *et al.*, 2008; Krasik *et al.*, 2008), and the use of exploding wires as substitutes of explosives in the generation and study of blast waves (Ram & Sadot, 2012; Liverts *et al.*, 2015). Also, carefully choosing the exploding wire parameters implies that some states of matter can be experimentally observed, such as their liquid state (Kuskova *et al.*, 1997), and therefore material properties of metals could be compared with theoretical predictions (DeSilva & Katsouros, 1998; Beilis *et al.*, 2009; Sheftman & Krasik, 2010).

To reach conclusions on the resulting plasma of an exploding wire, a fundamental parameter is the energy density deposition from the electrical circuit into the wire-plasma system. This energy deposition is very sensitive to the electrical current rate, as it has been demonstrated in previous experiments (Sarkisov *et al.*, 2004). To be able to perform measurements on the energy deposition, the most direct way is the use of voltage and current signals on the wire

Address correspondence and reprint requests to: G. Rodríguez Prieto, Universidad de Castilla-la Mancha, I.N.E.I., 13071, Ciudad Real, Spain. E-mail: gonzalo.rprieto@uclm.es

experimentally measured. Combination of these measurements with radial expansion dynamics allow for the exploration of the plasma parameters, so the comparison of experimental and simulated electrical waveforms are used frequently as benchmarks of codes and their conductivity models, therefore many examples can be found in the literature (Gurovich *et al.*, 2004; Beilis *et al.*, 2008; Stephens & Neuber, 2012).

In this work, we present the results for exploding wires of different metals with a current rate below 12 A/ns in atmospheric air. This value indicates a slow current rate in comparison with other works already published, where their current rates could be as large as 500 A/ns (Sheftman & Krasik, 2010). Experiments and simulations that show a complex interplay between the energy absorption and the current density are also presented in this work. They show an excellent agreement between the theoretical and experimental waveforms of the voltage and current values.

This paper is structured as follows. After this introduction, the experimental setup and numerical methods are explained in the two following sections. Experimental and simulation results are presented later, and a last section of conclusions ends this work.

2. EXPERIMENTAL SETUP AND METHODS

Experiments were performed with the ALEX system (Alambre Explosivo, in Spanish), a typical exploding wire setup, formed by a two capacitors bank (1.13 μF, 40 nH each) connected in parallel with a high-voltage source. A wire is attached in series between the spark-gap and the ground, having an inductance of 140 nH. Wires are of fixed length (3 cm) and surrounded by atmospheric air, but with different metals and diameters; see Table 1. Heat content data that are presented in the table had been obtained from Pankratz and Mrazek (1983). The initial voltage of the capacitor bank varied from 10 to 25 kV (in steps of 5 kV).

In Figure 1, the equivalent electrical circuit of the setup is shown, where the total inductance of the capacitors has been enclosed as a single component. Measurement of the time evolution of the energy delivered by the circuit to the wire has been obtained by recording the signals from a resistive voltage divider and a Rogowsky coil, placed in the locations indicated in Figure 2. Also the plasma radial expansion is

Table 1. *Metals, diameters, and heat content at melting and boiling points for the total mass of the wires employed in these experiments*

Metal	Diameter (μm)	H_{melt}–H_{298} (J)	H_{boil}–H_{298} (J)
Silver (Ag)	250	21.6	188.9
Molybdenum (Mo)	100	19.7	124.5
Copper (Cu)	50	1.4	13.0
	100	5.7	52.1
Tungsten (W)	100	13.8	94.8

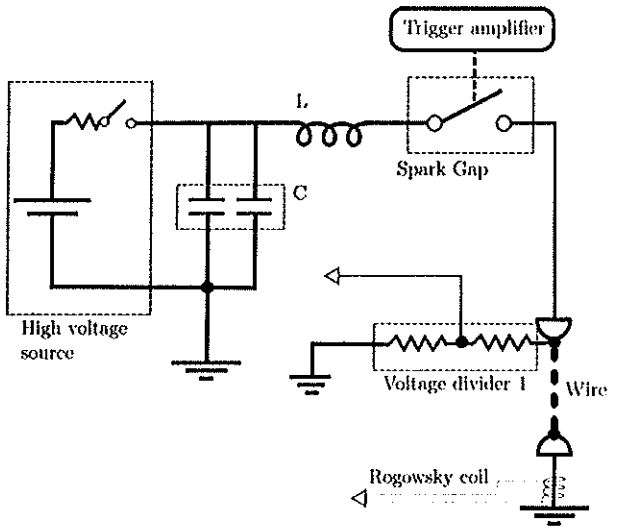

Fig. 1. ALEX electrical scheme. **L** and **C** mark the circuit inductance and capacitance, respectively. White arrows signal the BNC connections to the Faraday cage.

simultaneously measured as a function of time during the wire explosion time. Electrical probes has been designed and calibrated in our laboratory. The signals are transmitted through coaxial cables to the oscilloscopes, shielded against electromagnetic noise in a Faraday cage. Numerical integration of the Rogowsky signals gives the current that flows through the wire. To observe the plasma expansion, a streak image system was focused on the wire for recording the self-emitted plasma light. A fast photodiode, directed toward the wire, was used for the synchronization of the electrical signals with the optical images of the streak system; see Figure 2 for the scheme of the experimental setup.

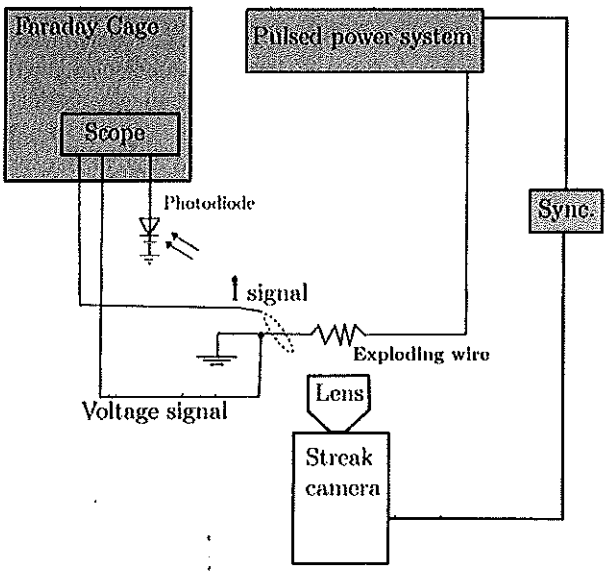

Fig. 2. Scheme of the experimental setup.

Recorded signals from the voltage divider correspond to the sum of the exploding wire voltage drop plus that of the electrodes and connections in series with the wire. In order to remove from the signals the unwanted voltage drop, that is, that of electrodes and connectors, a common practice is to use an *ad-hoc* approximation of the behavior of this part of the circuit by just a constant inductance. Thus, the voltage across the wire is obtained as the difference between the measured voltage and that of the modeled inductance.

We have instead used a different approach. As a matter of fact, the late oscillatory part of the signal (late in time, after formation and evolution of the plasma) is well fitted by two constant circuit elements, one inductive and other resistive. Note that the inductance and resistivity of the fitting are taken at latter times in the wire explosion, after its disappearance and they are different from the initial values. Therefore, the voltage drop on the wire is obtained by subtracting, from the measured signal, the previous fit. As an example, in Figure 3, we show the result of this procedure for a tungsten wire with a diameter of 100 μm and initial voltage of 15 kV. Further, the numerical simulation, which is described below, supports this approach.

From voltage and current across the exploding wire, we obtain the electrical power and the energy delivered to the wire. Furthermore, assuming cylindrical symmetry, the combination of the electrical current data with the radial expansion of the plasma, leads to a lower limit for the wire resistivity as a function of time obtained as (Rodríguez Prieto *et al.*, 2016):

$$\mu \leq \mu_{\min} = \frac{\Delta V S_w}{I l_w}, \tag{1}$$

where ΔV is the measured voltage along the wire, S_w is the wire section, I is the wire current, and l_w is the wire length.

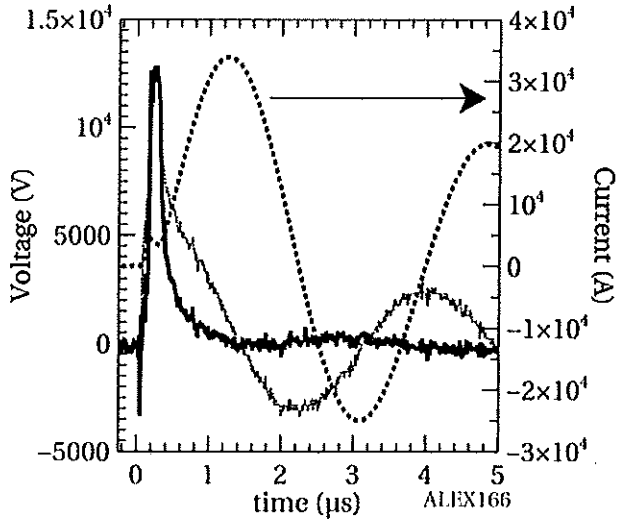

Fig. 3. Typical voltage, in wire (—) and the voltage divider (---), and current (-•-•-) signals for a tungsten wire, diameter 100 μm, with the capacitors bank charged at 15 kV.

From the recorded streak images, plasma radial evolution is obtained by a simple method. Plasma radial border is defined as the position where the intensity is 5% of the maximum recorded value on the streak image for each experiment. This is searched sequentially for each time instant and calibrated in space and time to obtain the final radial expansion that is then fitted by the function (Bennett, 1958):

$$r^2 = \sqrt{\frac{E_k}{\rho_{Air} l_w}} t, \tag{2}$$

where E_k is the kinetic energy of the plasma, that is, the fraction of the total energy absorbed employed by the plasma in its expansion, ρ_{Air} is the air density, and l_w is the wire length. The above procedure allows us to obtain the radial expansion with an error of 0.1 mm, meanwhile the error in determination of the time is 50 ns.

3. NUMERICAL METHOD

The experiment was simulated using a simplified, one-dimensional (1D) version of a full 3D multi-component plasma (neutrals, ions, and electrons), two temperature (one for electrons and other for ions and neutrals), Arbitrary Lagrangian–Eulerian, Finite Volume code (Bilbao, 2006). The code includes electrical resistivity, thermal conduction, magnetic diffusion, and an equation of state (EOS) from solid to plasma obtained from different sources and models, detailed a few lines later. We assumed cylindrical symmetry with only radial dependence in order to use the 1D version of the code.

The wire is coupled to the external circuit using (Rodríguez Prieto *et al.*, 2016):

$$\frac{d[(L_0 + L_b)I]}{dt} = \frac{Q}{C} - RI - \int_b \vec{E} \bullet d\vec{l}, \tag{3}$$

where Q is the charge of the capacitor bank, C is its capacity, L_0 and R are the inductance and the resistance of the concentrated elements of the circuit, respectively, L_b is the inductance calculated at the plasma boundary ("b" refers to the plasma boundary), $\vec{E}$ is the electric field along a path ($d\vec{l}$) on the plasma boundary (as seen in the frame fixed to the plasma), and I is the current.

Regarding the properties of the materials and the EOS, we have used the following approach. A Mie–Grüneisen EOS was used for solid and liquid, meanwhile both gas and plasma components (ions, electron, and neutrals) were simulated with an ideal gas EOS. The electrical resistivity and the thermal conductivity for solid and liquid states have been interpolated from the published data (Gray, 2016), for plasma state the Spitzer conductivity was used, while for gas state a trial and error method was used, as follows. Due to the lack of data on the conductivity of metallic gas, a linear

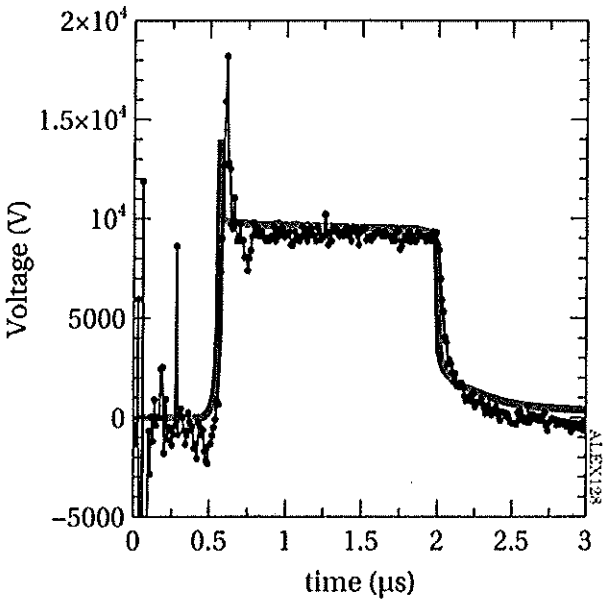

Fig. 4. Simulated (—) and experimental (-•-) voltage time evolution in a copper wire of 50 μm charged at 10 kV.

dependence with temperature was assumed, and then fitted until the simulated voltage was in a reasonable accordance with the measured experimental data. The previous model is necessary due to the fact that the electrical behavior of the circuit strongly depends on the electrical resistivity and the thermal conductivity of the wire.

As Figure 4 shows, simulation of the current and voltage on the wire as function of time for a 5 μm Cu wire, 10 kV charging voltage, reproduces well the features obtained in the experiments. Therefore we conclude that duration of the "dark pause" depends on the high resistivity of the wire after being vaporized but not sufficiently ionized to conduct large currents. Thus, electrical properties of the gas can be adjusted until an appropriated duration of this stage is achieved.

4. RESULTS

Typical streak images are similar in their features to the depicted in Figure 5. Plasma expansion growing with the charging voltage is clearly visible, as it is the similar duration of the light emission from the metallic plasmas in all the cases. Also, the differences on the wire evolution due to the different metals and masses of the wire are apparent in the streak pictures. Nevertheless, final plasma stage is similar in all the cases in our experiments because the surrounding medium is always atmospheric air. Synchronization of data from plasma radial expansion with electrical energy absorption of the wire–plasma system allows us to observe the

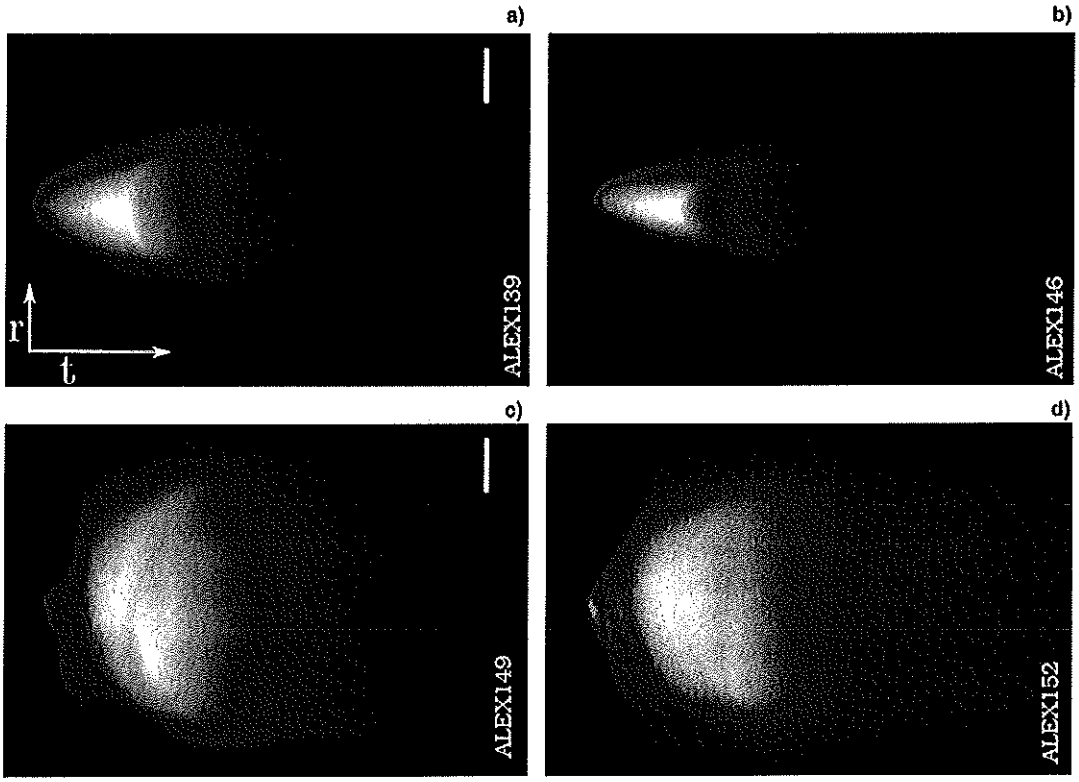

Fig. 5. Molybdenum (a, b) and silver (c, d) streak images with 25 and 10 kV charging voltage at left (a, c) and right (b, d), respectively. Bars indicate 9.6 mm and total time in horizontal dimension is 45 μs.

temporal relation between these two processes at different charging voltages.

At low initial charging voltages and for all the metals used in this work, except for tungsten, the energy transfer from the circuit to the wire, as measured by the electrical signals, is performed in two different steps. These two steps are defined by the appearance of light emission from the plasma in the streak images. Therefore, a first stage of energy absorption takes place before the plasma formation, in a pre-plasma formation stage, with an amount of energy absorption that can be an important percentage of the total absorbed energy. Plasma expansion begins in the second step, where the kinetic energy of the plasma is obtained from the partial absorption of the electrical energy delivered to the wire–plasma system.

Figure 6 illustrates this process of energy transfer and plasma expansion of a copper wire of 50 μm diameter charged at 10 kV. As the charging voltage increases, the time lapse between the two energy absorption steps is reduced, until the two steps merge into one. Therefore, with the maximum charging voltage of 25 kV the two steps are not distinguishable, as Figure 7 shows for the copper wire of 100 μm diameter.

Experiments performed with tungsten wire show a unique absorption stage even at low charging voltages. Also, due to the larger resistivity, the energy absorbed is higher than for copper; see Figure 8. Nevertheless, the maximum absorbed energy, almost 20 J, is similar to the heat content at melting,

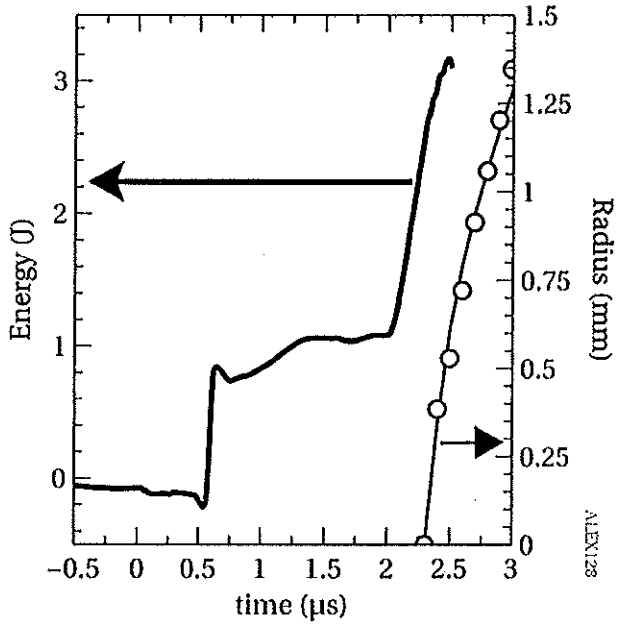

Fig. 6. Energy (—) and radial expansion of 50 μm copper wires (—o—) at 10 kV initial voltage charge. Hollow dots indicate experimental data and the line is the result of fitting them to the formula 2. Note the difference between the energy transferred to the wire and the heat content for the same wire, Table 1. This is an indication of the incomplete wire conversion into gas or plasma, also confirmed by simulations.

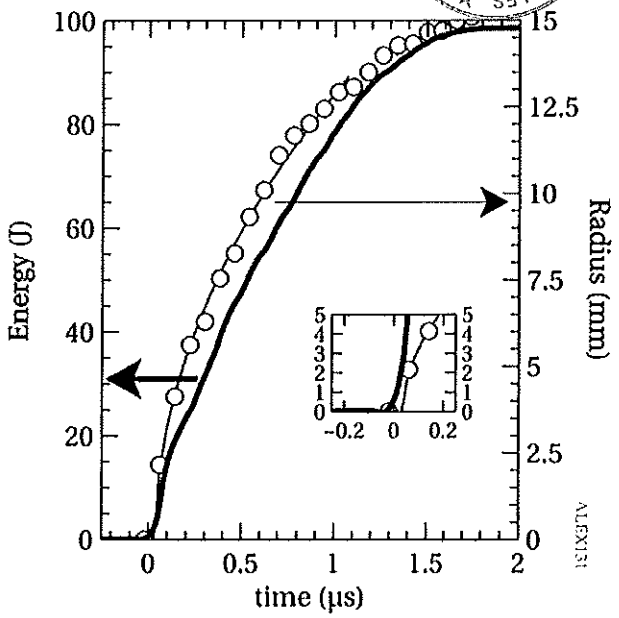

Fig. 7. Energy (—) and radial expansion of 100 μm copper wires(-o-) at 25 kV initial voltage charge. The inset shows the beginning of the expansion.

13.8 J, and far from the heat content at boiling, as Table 1 indicates. Both silver and molybdenum exhibit a general behavior similar to that observed using wires of copper or tungsten, except for the time delay between the beginning of electrical energy absorption and the plasma radial expansion.

At low initial voltage all metals exhibit a delay that decreases with the increasing in the charging voltage, but at larger voltages, some unexpected tendency emerges. For molybdenum the delay becomes negative, meaning that the main energy absorption is produced after the plasma

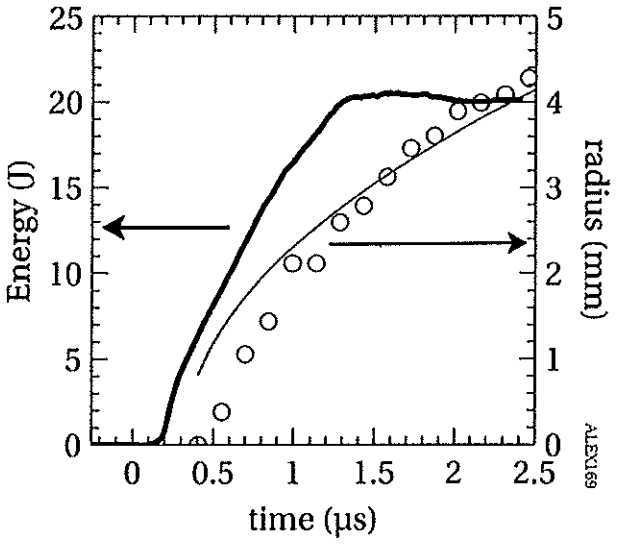

Fig. 8. Tungsten energy absorption and radial expansion with an initial charging voltage of 10 kV. Legend is the same that in Figures 6 and 7.

generation, defined as the moment when the self-emitted light reaches at least 5% of the maximum, as explained in Section 2 of this work. Meanwhile in the case of silver wires the observed delay oscillates around zero, as Figure 9 shows.

The behavior of the delay in both metals is not easy to understand. Based on simulations previously described, we found that in all cases, the delay (when present) occurs when the wire has been melted and vaporized into an almost non-ionized metallic gas state. Under this condition the resistivity is high and the current becomes very small, thus retarding the energy transfer and the posterior ionization processes. This energy transfer delay happens as long as the external resistance is smaller than the one of the metallic gas, thus is the latter the one that controls the electrical current value. Depending on the voltage, and the residual current, the joule heating will take a shorter or longer time to heat up the gas and provide the energy necessary to start the ionization process by thermal collision of the atoms, allowing for the gas transformation into plasma. Thus, the joule heating in this early time of the electrical discharge greatly influences the current density. As a matter of fact, it is the increment of the current density the reason of the reduction in the delay between the energy absorption and plasma generation whenever the charging voltages increased their values. When the charging voltage is high enough, the processes of melting, vaporizing, and ionization occurs in a short period of time, during the linear increase of the current with time, thus the radius of the plasma can be described by a self-similar approximation. Therefore, using (2), for the current density it can be written:

$$j \propto \frac{It}{r^2} = \sqrt{\rho_{Air} I_w} \frac{It}{\sqrt{E_k}}, \tag{4}$$

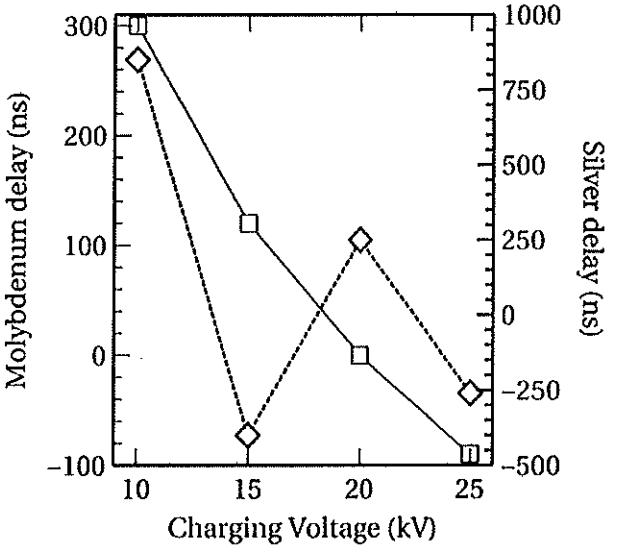

Fig. 9. Delay between the energy absorption and the beginning of plasma expansion at different charging voltages for Mo (—□—) and Ag(- -◊- -) wires.

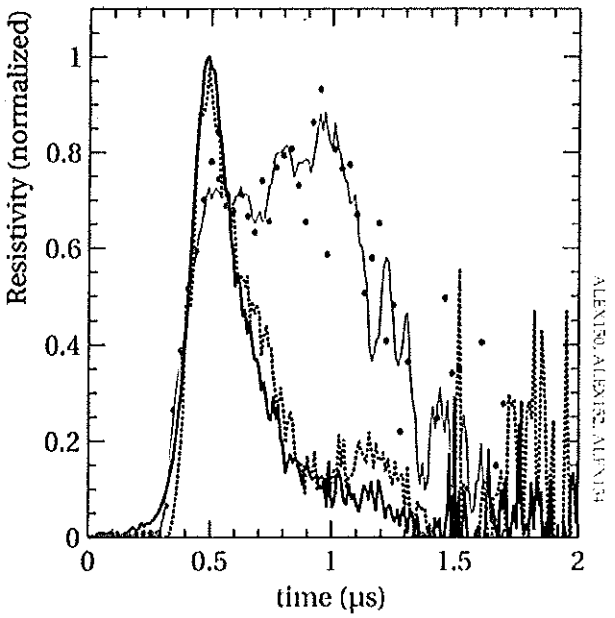

Fig. 10. Normalized resistivity of a silver wire of 250 μm diameter when the capacitor bank is charged with 10 (-•-), 15 (—), and 20 (---) kV.

where I is the current derivative. This means that the increase of the kinetic energy with the initial charging voltage, results in a reduction of the current density. So the delay between the electrical energy absorption and plasma creation can grow with the initial charging voltage, in a counterintuitive way, if the ratio between the current and the square root of the kinetic energy diminishes.

Simulations of the exploding wire support this interpretation. When, in the simulations, the plasma is not allowed to expand by means of artificial procedures (i.e., eliminating gas or plasma dynamics and its influence on the current density), the time between the gas and plasma formation reduces to zero.

The observed delay between the electrical energy absorption and plasma radial expansion is correlated with the measured lower limit of the resistivity as a function of time; see Figure 10. To better appreciate the differences on the time dependence of the resistivity, it has been normalized to the maximum achieved value. For a charging voltage of 10 kV, the resistivity increases until a quasi-constant plateau value, from where it decays with some peaks on the downward slope at about 1.5 μs after the beginning of the electrical discharge. While the charging voltage is settled in 15 and 20 kV, the time variation of the resistivity changes to a single peak, with different slopes for each charging voltage.

5. CONCLUSIONS

Variation on the synchronization between the electrical energy absorption of the plasma–wire system and the plasma formation has been observed experimentally, with values ranging from ≈0.0 to 2.0 μs, in the case of copper

wires. A non-intuitive relation for this delay had been observed for silver, as at 15 kV of charging voltage the delay changes its sign, interrupting the tendency to being reduced with the increase of the voltage observed with other metals. Both behaviors are understood in this work because of the interplay of the ratio between the current and the square root of the kinetic energy of the plasma.

Also the correlation of this delay with the shape of a lower limit to the wire resistivity has been measured. Two distinct time variations for the wire resistivity had been observed, namely a single peak with different slopes for each charging voltage, and a plateau of ≈0.7 μs if the charging voltage is 10 kV.

In conclusion, energy absorption in the exploding wire system for relatively slow current rates, with values under 12 A/ns, had been experimentally observed, and the difference in behavior with faster exploding wire systems (Sarkisov *et al.*, 2005*a*, *b*; Grinenko *et al.*, 2006) is attributed to the ratio between the current derivative passing through the wire and the square root of the kinetic energy of the plasma.

ACKNOWLEDGMENTS

This study has been partially supported by the Ministerio de Energía y Competitividad of Spain (grant no. ENE2013-45661-C2-1-P) and Junta de Comunidades de Castilla-la Mancha (grant no. EII-2014-008-P). The authors would like to thank Professor Roberto Piriz for his valuable comments and suggestions.

REFERENCES

Beilis, I.I., Baksht, R.B., Oreshkin, V.I., Russkikh, A.G., Chaikovskii, S.A., Yu Labetskii, A., Ratakhin, N.A. & Shishlov, A.V. (2008). Discharge phenomena associated with a preheated wire explosion in vacuum: Theory and comparison with experiment. *Phys. Plasmas* **15**, 013501. doi: 10.1063/1.2826434.

Beilis, I.I., Shashurin, A., Baksht, R.B. & Oreshkin, V. (2009). Density and temperature distributions in the plasma expanding from an exploded wire in vacuum. *J. Appl. Phys.* **105**, 033301. URL http://scitation.aip.org/content/aip/journal/jap/105/3/10.1063/1.3050343.

Bennett, F.D. (1958). Cylindrical shock waves from exploding wires. *Phys. Fluids* **1**, 347–352.

Bennett, F.D., Hefferlin, R. & Strehlow, R.A. (1969). *Progress in High Temperature Physics and Chemistry, Vol. II. High-Temperature Exploding Wires*. London: Pergamon Press.

Bilbao, L. (2006). A three-dimensional finite volume arbitrary lagrangian-eulerian code for plasma simulations. *AIP Conf. Proc.* **875**, 467–472. URL http://scitation.aip.org/content/aip/proceeding/aipcp/10.1063/1.2405990.

Chandler, K.M., Hammer, D.A., Sinars, D.B., Pikuz, S.A. & Shelkovenko, T.A. (2002). The relationship between exploding wire expansion rates and wire material properties near the boiling temperature. *IEEE Trans. Plasma Sci.* **30**, 577–587.

DeSilva, A.W. & Katsouros, J.D. (1998). Electrical conductivity of dense copper and aluminum plasmas. *Phys. Rev. E* **57**, 5945–5951.

Efimov, S., Fedotov, A., Gleizer, S., Gurovich, V.T.Z., Bazalitski, G. & Krasik, Y.E. (2008). Characterization of converging shock waves generated by underwater electrical wire array explosion. *Phys. Plasmas* **15**, 112703.

Gray, T. (2016). Photographic periodic table of the elements. http://periodictable.com Accessed on February 2016. URL http://periodictable.com.

Grinenko, A., Krasik, Y.E., Efimov, S., Fedotov, G. & Gurovich, V.T.Z. (2006). Nanosecond time scale, high power electrical wire explosion in water. *Phys. Plasmas* **13**, 042701.

Gurovich, V.T.S., Grinenko, A., Krasik, Y.E. & Felsteiner, J. (2004). Simplified model of underwater electrical discharge. *Phys. Rev. E* **69**, 036402.

Krasik, Y.E., Grinenko, A., Sayapin, A., Efimov, S., Fedotov, A., Gurovich, V.Z. & Oreshkin, V.I. (2008). Underwater electrical wire explosion and its applications. *IEEE Trans. Plasma Sci.* **3**, 423–434.

Kuskova, N.I., Tkachenko, S.I. & Koval, S.V. (1997). Investigation of liquid metallic wire heating dynamics. *J. Phys.: Condens. Matter* **9**, 6175–6184.

Liverts, M., Ram, O., Sadot, O., Apazidis, N. & Ben-Dor, G. (2015). Mitigation of exploding-wire-generated blast-waves by aqueous foam. *Phys. Fluids* **27**, 076103.

Nairne, E. (1780). An account of the effect of electricity in shortening wires. *Philos. Trans. R. Soc. Lond.* **70**, 334–337.

Pankratz, L.B. & Mrazek, R.V. (1983). Thermodynamic properties of elements and oxides. *Bur. Mines Bull.* **672**, 1–143.

Ram, O. & Sadot, O. (2012). Implementation of the exploding wire technique to study blast-wavestructure interaction. *Exp. Fluids* **53**, 1335–1345.

Rodríguez Prieto, G., Bilbao, L. & Milanese, M. (2016). Temporal distribution of the electrical energy on an exploding wire. *Laser Part. Beams* **34**, 263–269. URL http://journals.cambridge.org/articleS0263034616000069.

Sarathi, R., Sindhu, T.K., Chakravarthy, S.R., Sharma, A. & Nagsesh, K.V. (2009). Generation and characterization of nano-tungsten particles formed by wire explosion process. *J. Alloys Compd.* **475**, 658–663.

Sarkisov, G.S., Rosenthal, S.E., Cochrane, K.R., Struve, K.W., Deeney, C. & McDaniel, D.H. (2005*a*). Nanosecond electrical explosion of thin aluminum wire in vacuum: Experimental and computational investigations. *Phys. Rev. E* **71**, 046404.

Sarkisov, G.S., Struve, K.W. & McDaniel, D.H. (2004). Effect of current rate on energy deposition into exploding metal wires in vacuum. *Phys. Plasmas* **11**, 4573.

Sarkisov, G.S., Struve, K.W. & McDaniel, D.H. (2005*b*). Effect of deposited energy on the structure of an exploding tungsten wire core in a vacuum. *Phys. Plasmas* **12**, 052072.

Sasaki, T., Yano, Y., Nakajima, M., Kawamura, T. & Horioka, K. (2006). Warm-dense-matter studies using pulse-powered wire discharges in water. *Laser Part. Beams* **24**, 371–380.

Sheftman, D. & Krasik, Y.E. (2010). Investigation of electrical conductivity and equations of state of non-ideal plasma through underwater electrical wire explosion. *Phys. Plasmas* **17**, 112702.

Stephens, J. & Neuber, A. (2012). Exploding-wire experiments and theory for metal conductivity evaluation in the sub-eV regime. *Phys. Rev. E* **86**, 066409.

Stephens, J.C., Neuber, A.A. & Kristiansen, M. (2012). Simulation of an exploding wire opening switch. *2012 14th International Conference on Megagauss Magnetic Field Generation and Related Topics (MEGAGAUSS)*, 1–4. doi: 10.1109/MEGAGAUSS.2012.6781418.

[3] ENVIADO, EN PROCESO DE REVISION

IEEE TRANSACTIONS ON PLASMA SCIENCE

On the Measurement of the Resistivity in an Exploding Wire Experiment in Air

Luis Bilbao, Gonzalo Rodríguez Prieto

Abstract—**The explosion of a metallic wire due to a large electrical current has been used for a long time as a probe for studying the states of metals that are difficult to reach with other experimental methods. Among the measured magnitudes, the electrical current and voltage waveforms are very important because many characteristics of the metal in the wire can be derived from these waveforms.**

Due to experimental constraints, not always the voltage drop in the wire can be directly measured. Therefore, the measured voltages need to be process by counting the part of the circuit which is simultaneously included with the wire. Such correction is made using a lumped circuit model for the inductance and resistance of the electrical circuit attached to the wire. This lumped model is also used in the exploration of the variation in time of the wire resistivity.

Here, we discuss in detail the validity of such approach, and we show that due to the variation in time of the current density distribution on the wire, a model of lumped elements will not provide accurate values for the wire resistivity, specially in gas and plasma states, due to the diffusion and movement of the current that produce a large variation of the magnetic flux inside the wire. A better approach is the use of the Faraday's law of induction applied on a path along the border of the wire. In particular, from an alectrical point of view, exploding wire experiments in atmospheric air have the boundary of the wire well defined, for the current does not circulate beyond that border. As this border evolves through the different states (solid, liquid, gas, and plasma) of scientific and technical interest, it is possible to estimate the resistivity of the metal in those states in a more precise way than using a lumped model.

Index Terms—**Circuit analysis, metals, atmospheric-pressure plasmas, exploding wire, resistivity.**

I. Introduction

WHEN a large electrical current passes through a metallic wire of the proper dimensions, typically 100 μm of diameter and centimeters length, the metallic wire is heated rapidly by Joule effect, becoming liquid, then gas, to later be transformed in plasma. This system is called exploding wire, and it is well known to science since a long time [1].

It had been used since then in multiple endeavors, because the rich phenomena that can be accessed with it. Broad examples of the use of exploding wire are the general use as generator mechanism for blast waves [2] or the better understanding of the fuse dynamics through experiments like in the work of Vermij [3]. Exploding wire systems can also be used for important industrial or military applications, like in the preparation of metallic nano-powders reviewed by Kotov et al. [4], or the study of the mitigation of blast waves by foam, through the use of a surrogate setup, as in the recent work of Liveets et al. [5].

In order to create the high current necessary for this phenomenon, large capacitors and high voltages are necessary in the electrical circuit that delivers the current to the wire load. Therefore, and adding to these elements, the circuit inductance and resistance, a model for the exploding wire as a RLC circuit with the wire as a circuit load can be used for understanding the voltage and current signals recorded in experiments. Do to experimental constrains, sometimes the voltages probes are not exactly placed between the wire extremes, but separated by fixed circuit elements from them. For example, as described in the experimental works [6]–[10]

Therefore, it is important to perform a correct modeling of the wire load, in order to isolate the voltage between the wire extremes from the voltage recorded in the experiments. Usually the wire is modelled as a lumped element, so the resistance of the wire, and in latter stages, of the plasma, can be measured indirectly using the voltage signals, as in [11]–[14].

Despite of the broad use of the lumped model for the wire, during the time when the diffusion of the electrical current is important or when a large variation of the resistivity occurs within the wire, the lumped model description is not accurate. Therefore, we present here a different approach to the description of the circuit. It is based on the derivation of the circuit equation by means of the Faraday's law of induction.

II. Electrical Circuit

The experimental setup of ALEX (ALambre EXplosivo, exploding wire acronym in Spanish), the exploding wire experiment motivating this work, including an optical streak camera, has been described in a previous work [15]. Nevertheless, it is worth to recall a description of its electrical circuit and the associated probes here. The capacitor bank, two parallel Castor oil capacitors of 1.1 μF each, is charged by a high voltage source of a maximum voltage of 65 kV. Upon arrival to the desired nominal voltage, the high voltage source is disconnected from the circuit, and the spark gap is triggered (see fig. 1). Later on, when the spark gap switch is fully closed, the circuit is equivalent to a RLC circuit plus the wire load.

The use of lumped element model for the exploding wire is not always the best approach. The discharge on the wire produces a current that diffuses due to the resistivity. During this stage, it is impossible to define separately a resistance and an inductance as lumped parameters of the circuit [16].

L. Bilbao is with Universidad de Buenos Aires, Argentina.
G. Rodríguez Prieto is with Universidad de Castilla-La Mancha, Spain and INEI, Ciudad Real, Spain
Manuscript received ...; revised ...

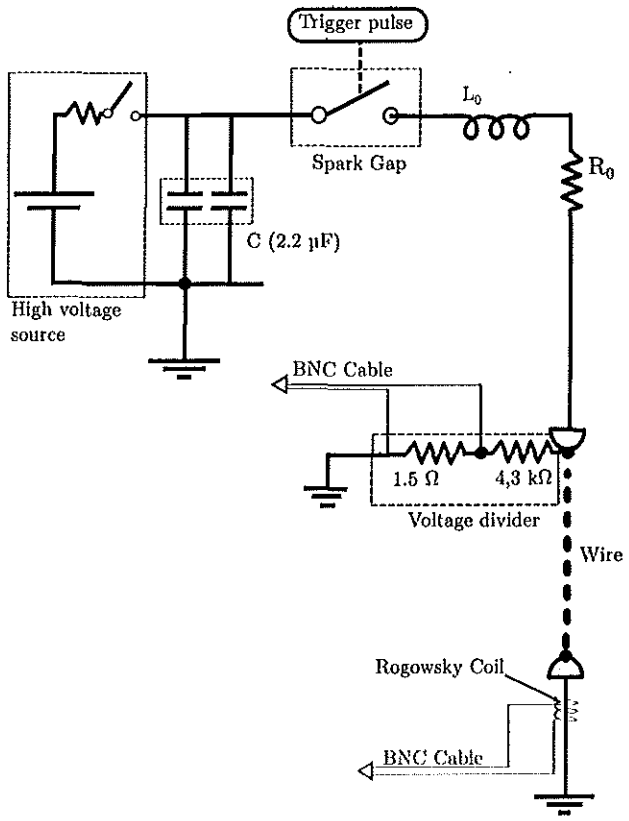

Fig. 1. ALEX electrical scheme. R_0, L_0 and C mark the circuit resistance, inductance and capacitance, respectively. White arrows indicate the BNC connections to the oscilloscope.

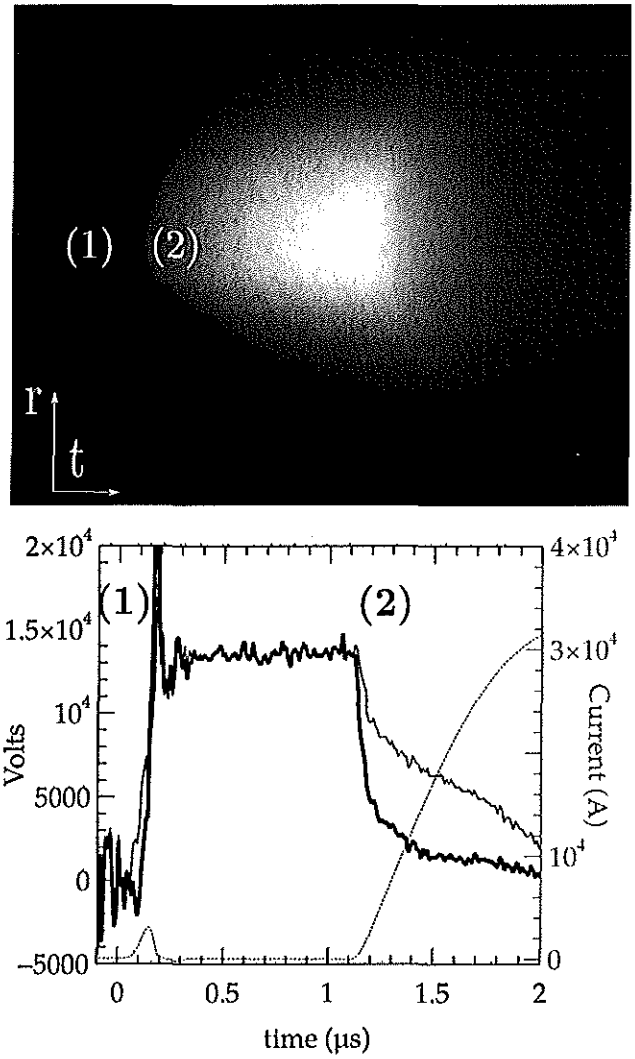

Fig. 2. (Color Online) In the upper panel, exploding wire streak image. Time in the horizontal axis is 20 μs, and space in the vertical axis, 2.4 cm. Down panel shows the voltage through the wire (thick full line), the signal of the voltage divider (thin full line), and the current (green dotted line). Numbers in both panels corresponds to the same moments in both the streak image and the signals. Charging voltage was 15 kV with a wire diameter of 50μm

Notwithstanding this fact, lumped element models for the wire have been used for more than 50 years [7], [17]–[19], and therefore it is a common practice to refer to a wire resistance and inductance. The practical use of such approach is the obtention of the resistivity of the metal as a function of time from the electrical signals and the wire/plasma radius evolution. To do so, a homogeneous evolution in density and resistivity is assumed. An example which clearly states this lumped model for the wire is the work of Sasaki et al. [11].

The above hypothesis is not usually well justified in all the stages of the exploding wire evolution. For example, under appropriate conditions the dark pause can last several μs. After an initial rise, the current drops almost to zero while the full voltage is across the wire. This low current stage lasts for a given time until a second surge of the current develops, see fig. 2.

The elapsed time between the first and the second surges of the current will depend on the resistivity of the wire and the distribution of the current. After the first current surge, the wire melts and vaporizes. When part of the wire vaporizes, the sudden increase of the wire resistivity produces a sharp drop in the current. Although small, a residual current continues flowing and heating up the wire and the change of the state of the metal progresses through the wire. This means that different states (liquid, liquid/gas, and gas) may coexist in the wire, having very large difference in their resistivities. Therefore, assuming a lumped model, no reliable information on the wire resistivity can be extracted from measurements due to the average concept of the resistance.

Resuming, the dark pause stage is characterized by a variation of the current in a time period comparable to the diffusion time and a large variation of the metal resistivity. Thus, a lumped element model of this stage will not be of sufficient accuracy to evaluate the Joule heating contribution to metallic gas. A better approach is described below.

III. Circuit Equation

In order to model the electrical circuit, it is divided into three distinct parts: a) capacitors, cables, electrodes and connections, b) the spark gap, and c) the exploding wire.

Part a) can be modeled with a RLC lumped element model, as it is experimentally seen using a short circuit. In our case, the wire is removed and the cathode is displaced until it touches the anode, i.e. no short circuit element is added. The measured current derivative can be perfectly fitted by a dumped cosine at the later stage where the voltage drop across the spark gap is zero. The values of the lumped elements R_0 and L_0 are obtained from the fit with high precision, see fig. 3 (the capacitance, C, is provided by the manufacturer). The difference between the fitted RLC signals and the actual signals that is seen at the beginning of the signal (the first μs in fig. 3) is an oscillation due to the finite closure time of the spark gap.

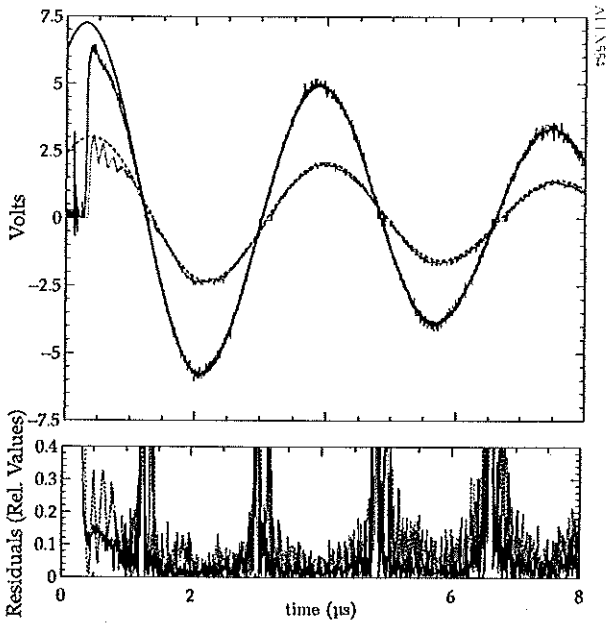

Fig. 3. (Color Online) ALEX short circuit waveforms, as thin dotted lines, and their approximation (top panel) with the residua (down panel) when charged at 10 kV. Continuous (black) lines correspond to the Rogowsky probe and dashed (green) lines belong to the voltage divider. Note the large value of the residua at the beginning of the discharge, when an oscillation is produced by the finite closure time of the spark-gap.

Due to the fact that the closure time of the spark gap is much shorter than the period of the discharge, the behavior of the spark gap, part b), is well modeled by a variable voltage drop. For the voltage variation across the spark gap, $V_{sg}(t)$, we have used [20]

$$V_{sg}(t) = \frac{2V_0}{1+\exp(t/\tau)}, \tag{1}$$

where V_0 is the initial charging voltage of the capacitor, τ the spark-gap closure time, and $t = 0$ corresponds to the trigger of the spark gap.

In order to obtain the voltage drop on the wire, in our experiment we have to take into account that the position of the voltage divider is at the connexion between the anode and the wire. Therefore, the measured voltage drop, V_{probe}, is the sum of the voltage drop across the exploding wire, V_{ew}, plus the voltage drop in the cathode and connexions. As can be seen in the short circuit signals of fig. 3, when no wire is present the measured voltage (i.e. the drop in the cathode) is perfectly fitted by a lumped resistance, $R_{cathode}$, and inductance, $L_{cathode}$. These values (different from R_0 and L_0) are then used in a discharge to obtain the voltage drop across the exploding wire, from the measured V_{probe} and the current derivative (dI/dt), as

$$V_{ew} = V_{probe} - R_{cathode} I - L_{cathode} \frac{dI}{dt},$$

where the current I is obtained by numerically integrating dI/dt.

For part c), we assume that current is distributed in the space, that is, the current flows through different paths between the electrodes.

Usually Kirchhoff's circuit laws are used to solve the current and voltage in an exploding wire experiments, regardless that it is only valid for a lumped element mode. When the current is spatially distributed a more precise way to write the circuit equation is by means of the Faraday's law of induction, along a closed path across the full circuit, that goes through the lumped elements, the spark gap, and the exploding wire as

$$\frac{d\Phi}{dt} = -\oint \mathbf{E}' \cdot d\mathbf{l}, \tag{2}$$

where Φ is the magnetic flux enclosed by the path, and $\mathbf{E}'$ the electric field in a system fixed to the path ($d\mathbf{l}$). The path may be a material or an immaterial one. Also, it may be a fixed or a mobile path relative to the lab system. In any case the electric field $\mathbf{E}'$ is evaluated in a system fixed to the path, not to the lab.

Along the part modeled with the lumped element model, the path is unique (i.e., the elements have no thickness), while on the exploding wire (whether on its initial state or during its evolution) any path that connect the electrodes may be used.

The integration of the electric field on the part that is modeled by a lumped element is straight forward, because it holds that

$$\int_{inductance} \mathbf{E}' \cdot d\mathbf{l} = L_0 \frac{dI}{dt}, \tag{3}$$

$$\int_{resistance} \mathbf{E}' \cdot d\mathbf{l} = R_0\, I, \tag{4}$$

and

$$\int_{capacitor} \mathbf{E}' \cdot d\mathbf{l} = -\frac{Q}{C}, \tag{5}$$

where Q is the charge.

On the other hand, as it was mentioned above, the spark-gap can be modeled by a variable voltage, that is

$$\int_{spark-gap} \mathbf{E}' \cdot d\mathbf{l} = V_{sg}(t). \tag{6}$$

Finally, for the exploding wire it is necessary to choose a path that connects the electrodes. For example, using path a as shown in fig. 4, left panel, (2) becomes

$$\frac{d\Phi_a}{dt} + \int_a \mathbf{E}' \cdot d\mathbf{l} = \frac{Q}{C} - R_0 I - L_0 \frac{dI}{dt} - V_{sg}(t), \tag{7}$$

where Φ_a is the magnetic flux enclosed by the circuit that is formed by the path a.

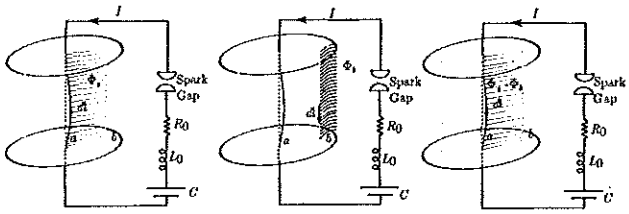

Fig. 4. (Color Online) ALEX integration paths with the magnetic flux indicated. Left panel through the center of the plasma, central panel through the outer border of the plasma, and in the right panel, the flux difference between previous paths.

Any other path may be used as well, including a mobile path along the wire boundary (see fig. 4, central panel), in which case we have

$$\frac{d\Phi_b}{dt} + \int_b \mathbf{E}' \cdot d\mathbf{l} = \frac{Q}{C} - R_0 I - L_0 \frac{dI}{dt} - V_{sg}(t). \quad (8)$$

Clearly, (7) and (8) produce the same voltage drop in the circuit, since Faraday's law along a closed path formed by a and b, gives

$$\frac{d\Phi_a}{dt} + \int_a \mathbf{E}' \cdot d\mathbf{l} = \frac{d\Phi_b}{dt} + \int_b \mathbf{E}' \cdot d\mathbf{l}. \quad (9)$$

(see fig. 4, right panel).

The above relationship also shows an important fact when diffusion of the current is the dominating phenomenon: it is impossible to meaningfully define separately a resistance and an inductance of the wire as lumped parameters in the circuit [16]. This can be better seen using the Ohm law in a system fixed to the wire material, where the electric field is evaluated, that is

$$\mathbf{E}' = \rho \mathbf{j}, \quad (10)$$

where ρ is the resistivity and $\mathbf{j}$ the current density, then (9) becomes

$$\frac{d\Phi_a}{dt} + \int_a \rho \mathbf{j} \cdot d\mathbf{l} = \frac{d\Phi_b}{dt} + \int_b \rho \mathbf{j} \cdot d\mathbf{l}. \quad (11)$$

Equation (11) shows that the inductive (first terms in each side) and the resistive parts (second terms in each side) depend on the path, thus a unique definition of the total inductance and resistance of the wire can not be made. Therefore, the use of a load resistance and inductance to simulate the exploding wire is, at best, an approximation that should be used with care.

Although (7) and (8) can be used indistinctly, we have choose the path b along the border of the wire. In our devices, the returning electrical path is a conducting plate separated by a distance d from the axis of the wire. Assuming cylindrical symmetry, the azimuthal magnetic field B outside the border of the wire is

$$B = \frac{\mu_0 I}{2\pi r_b},$$

where r_b is the radius of the border and I the current circulating through the wire

$$I = \int \mathbf{j} \cdot d\mathbf{S}.$$

Note that the electrical current does not circulate beyond the wire border because of the air surrounding the wire. Thus, the calculation of the magnetic flux enclosed by a path along the border of the wire and the returning plate, can be simply calculated as

$$\Phi_b = L_b I.$$

being L_b a geometrical relationship, that in a case with cylindrical symmetry is written as

$$L_b \equiv \frac{\mu_0 l}{2\pi} \cosh^{-1}\left(\frac{d}{r_b}\right), \quad (12)$$

being l the length of the wire.

Since the voltage drop across the wire is

$$V_{ew} = \frac{Q}{C} - R_0 I - L_0 \frac{dI}{dt} - V_{sg}(t), \quad (13)$$

after some rearrangement, the circuit equation (8) reads

$$\frac{d(L_b I)}{dt} + \int_b \rho \mathbf{j} \cdot d\mathbf{l} = V_{ew}. \quad (14)$$

In order to solve the circuit equation, the current density, the resistivity and the movement of the boundary layer are needed. Note that L_b cannot be seen as the wire inductance, since further magnetic flux that varies with time is inside the wire. Similarly, the second term of the left hand side cannot be replaced by a lumped resistance voltage drop in the form $R_b I$. If this were the case, the terms R_b and dL_b/dt will be undistinguished between them in the electrical signals, thus a unique solution for R_b can not be experimentally obtained. This fact has been pointed out by Fridman [21] in the sense that time evolution of the resistance and the inductance obtained from the oscillograms of current and voltage is not a single-valued problem.

Actually, there is no need of calculating a wire inductance or resistance in order to solve the circuit equation. Instead, a "boundary inductance" (L_b) and a "boundary resistive voltage drop" ($\int_b \rho \mathbf{j} \cdot d\mathbf{l}$) are sufficient. Inside the wire, the Faraday's law of induction may be further used for deriving its structure.

The set of equations (14) and (12) plus the exploding wire radial evolution, together with the initial conditions

$$Q(t=0) = CV_0\ ; \qquad I(t=0) = 0\ ; \qquad \frac{dI}{dt}(t=0) = 0$$

solves the circuit.

IV. Numerical Simulation

The aim of the numerical simulation is to help to understand the influence of the magnetic flux variation and the nonuniform resistivity inside the wire in the interpretation of electrical signals.

During the dark pause the drop of the current indicates an important increment of the resistivity, suggesting that the wire has been vaporized. The variation of resistivity of the copper until the boiling temperature [22] is not enough to explain the observed drop.

The end of the dark pause occurs when the metallic gas is ionized and the current is re-establish through the wire. Note

that for simplicity we call "wire" to either state, that is solid, liquid, gas or plasma.

In order to show this ideas, a 1D numerical code has been used to simulate the exploding wire dynamics. A key hypothesis in this approach is the symmetry of the wire evolution, during the time of interest, that is the dark pause in the present work. We assumed cylindrical symmetry with only radial dependence. In this way the plasma expansion can be approximate by a 1D system where the spatial coordinate corresponds to the radius. To the purpose of the present analysis, the symmetry of the wire observed during the dark pause by means of streak and framing pictures, allows us the use of a 1D code where magnitudes depend only on the radial coordinate.

Therefore, we have adapted a previous developed 3D code [23], that has been used to simulate different physical problems such as double-base chemical propellant combustion, ignition and propagation of a thermonuclear detonation wave, and, the development of the Kelvin-Helmholtz (KH) instability in the magnetopause. In the present version, a Mie-Grüneisen equation of state for solid and liquid was used, and the ionization state was obtained from a Saha equation. This is justified in the fact that our focus is the study of the dark pause, that ends when a cold plasma is formed. The successive evolution of the plasma at higher temperatures is out of the scope of this study.

The electrical resistivity of copper is readily available for solid, liquid [22] and plasma states, but not for the gas state. Anyway, an order of magnitude value can experimentally be obtained from the "boundary resistive voltage drop" mentioned above. Based on the measured values, using the numerical simulation we were able to reproduce fairly well the electrical signals, using a rough estimate of the copper gas resistivity, ρ_{gas}, including a linear variation with temperature, as

$$\rho_{gas} = 4\ m\Omega\ m\left[1 + 0.00045\left(T - T_{boil}\right)\right], \qquad (15)$$

where T is the gas temperature in Kelvin, and $T_{boil} = 2940$ K the boiling temperature of copper. The above estimate is intended only to illustrate the differences that may arise when a resistive and inductive lumped model is used for the exploding wire. It cannot be taken as a precise value of the copper gas resistivity.

A fairly good reproduction of the electrical signals were obtained by solving the numerical code coupled to the circuit equation, using the values of our experiment, $C = 2.2$ μF, $L_0 = 142$ nF, $R_0 = 5$ mΩ, $V_0 = 15$ kV, copper wire 50 μm in diameter and 30 mm long. Fig. 5 shows the voltage drop in the wire (simulated and measured) as a function of time, with the state of the outer layer of the wire over-imposed, as it evolves from solid to plasma. Note that the state in the inner part of the wire may differ from the external layer. Different states may coexist in the radial direction that evolve with different time scales.

V. Measurement of the Resistivity

It is a common practice to obtain a value of resistance, R, from the electrical signal, by subtracting the "inductive" part

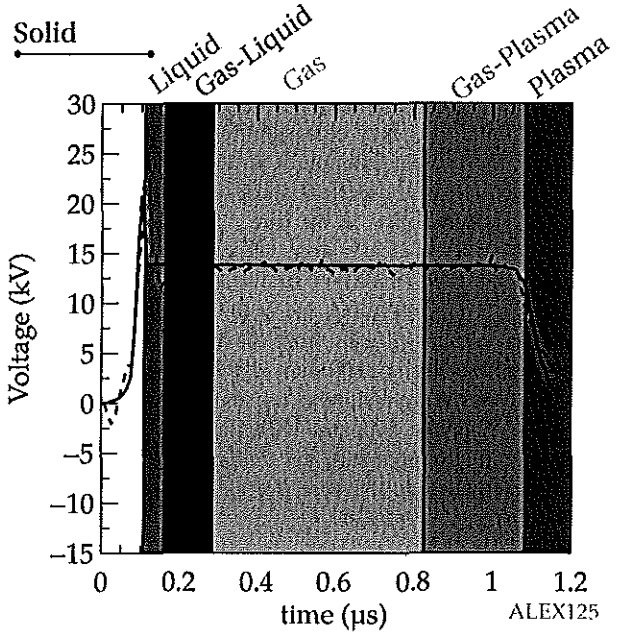

Fig. 5. (Color online) ALEX voltage waveforms (calculated full line, measured, dashed line) with the states of the outer shell of the wire clearly indicated, from a copper wire with a diameter of 50 μm and with capacitors charged at 15 kV.

from the voltage drop on the exploding wire as

$$R = \frac{V_{ew} - \frac{d(LI)}{dt}}{I}, \qquad (16)$$

where V_{ew} is the voltage drop across the exploding wire, L the inductance obtained from the geometrical form of the exploding wire, and I the current circulating on it.

From (16) a mean resistivity my be inferred as

$$\langle\rho\rangle = \frac{RA}{l}, \qquad (17)$$

where l is the length and A the section of the wire.

Comparing with (14) and assuming cylindrical symmetry it follows that

$$\langle\rho\rangle = \rho_b \frac{j_b}{\langle j\rangle}, \qquad (18)$$

where $\langle j\rangle = I/A$ is the mean current density. Clearly, when no magnetic flux variation is inside the wire (this implies that there is no current diffusion, either), the above relationship gives a reasonable mean value since $\rho j = const$ along the radius, unless large variation of the resistivity occurs inside the wire (for example, when different states coexist), in which case, a mean value has no significance.

In order to show the above problems, from the simulated electrical signals, a mean resistivity was obtained from (17) and compared to a mean resistivity, $\overline{\rho}$, over the radial position

$$\overline{\rho} = \frac{1}{r_b}\int_0^{r_b} \rho\left(r\right) dr.$$

Other mean values may be defined as well, but the aim of this paper is to show the difficult of interpreting (17) as a

representative value.

The percentage difference $(\langle\rho\rangle - \overline{\rho})/\overline{\rho}$ is plotted in figure 6. As can be seen, the difference varies up to $\pm 100\%$. From this result it is clear that the resistivity experimentally obtained from (16) and (17) may considerably depart from the actual value. In the present example it is due to two main factors: a) the diffusion of the current and b) the different states that simultaneously coexists in the wire.

The effect a) is clearly seen when the current varies in a characteristic time smaller or similar to the diffusion time, as it happens at the beginning and at the end of the dark pause. When the current diffuses from the boundary to the center, the current density is maximum at the border (i.e. $j_b > \langle j \rangle$) producing an overvalued mean resistivity, as can be seen from (18). The opposite happens when the current diffuses from the center to the boundary, or similarly when the magnetic flux decreases inside the wire (for example, due to a sudden expansion).

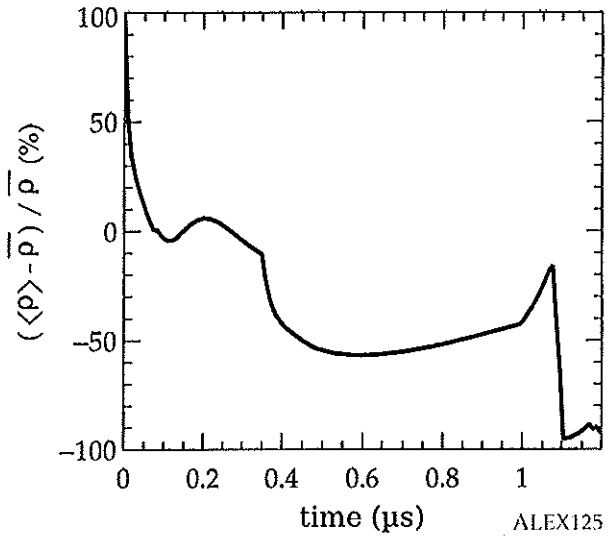

Fig. 6. Calculated resistivity deviation of the average from the mean. A copper wire of 50 μm diameter and 30 mm length and a charged voltage of 10 kV were used in the simulation.

The coexistence of different states that evolve during the dark pause, produce large difference in the resistivity (many orders of magnitude) across the wire making meaningless the concept of a mean resistivity. For example, in the example of fig. 6, the gas state of the outer layer coexists with the liquid-gas state of the central layer (not shown in the figure).

VI. Conclusions

The obtention of a resistivity from the experimental measurements of the electrical signals and the wire evolution, assuming a lumped element model as in (16) and (17), may give large difference relative to the actual resistivity, in particular when the current varies during a time comparable to the diffusion time, or when different states coexist inside the wire. Therefore, the use of lumped element model for the exploding wire is at best an approximation, that may be use with care.

If the study of the properties of the metal as a function of temperature and density is seek, a better strategy would be to obtain the resistivity of the outer layer of the wire, by measuring the "boundary resistive voltage drop". The external part of the wire varies its state from solid to plasma, thus, in principle, the time variation of the resistivity corresponding to different states may be studied. The resistivity of the outer layer can be estimated, as long as the current density is known.

There is no need to estimate the resistivity of the inner part, nor its mean value on the wire. It is enough to study the outer layer, and, if possible, by also measuring temperature, density and current density.

References

[1] E. Nairne, "An account of the effect of electricity in shortening wires," *Philosophical Transactions of the Royal Society of London*, vol. 70, pp. 334 – 337, 1780.

[2] K. Oshima, "Blast waves produced by exploding wire," Aeronautical Research Institute, University of Tokio, Tech. Rep. 358, 1960.

[3] L. Vermij, "The voltage across a fuse during the current interruption process," *IEEE Transactions on Plasma Science*, vol. 8, no. 4, pp. 460 – 468, 1980.

[4] Y. A. Kotov, "Electric explosion of wires as a method for preparation of nanopowders," *Journal of Nanoparticle Research*, vol. 5, no. 5, pp. 539 – 550, 2003.

[5] M. Liverts, O. Ram, O. Sadot, N. Apazidis, and G. Ben-Dor, "Mitigation of exploding-wire-generated blast-waves by aqueous foam," *Physics of Fluids*, vol. 27, no. 7, p. 076103, 2015.

[6] R. J. Thomas and J. R. Hearst, "An electronic scheme for measuring exploding wire energy," *Instrumentation and Measurement, IEEE Transactions on*, vol. 16, no. 1, pp. 51 – 62, 1967.

[7] A. W. DeSilva and J. D. Katsouros, "Electrical conductivity of dense copper and aluminum plasmas," *Physical Review E*, vol. 57, no. 5, pp. 5945 – 5951, 1998.

[8] D. B. Sinars, M. Hu, K. M. Chandler, T. A. Shelkovenko, S. A. Pikuz, J. B. Greenly, D. A. Hammer, and B. R. Kusse, "Experiments measuring the initial energy deposition, expansion rates and morphology of exploding wires with about 1 ka\wire," *Physics of Plasmas*, vol. 8, no. 1, pp. 216 – 230, 2001.

[9] K. M. Chandler, D. A. Hammer, D. B. Sinars, S. A. Pikuz, and T. A. Shelkovenko, "The relationship between exploding wire expansion rates and wire material properties near the boiling temperature," *IEEE Transactions on Plasma Science*, vol. 30, no. 2, pp. 577 – 587, 2002.

[10] S. Sahoo, A. K. Saxena, T. C. Kaushik, and S. C. Gupta, "Effect of energy deposition rate on plasma expansion characteristics and nanoparticle generation by electrical explosion of conductors," *High Energy Density Physics*, vol. 17, no. B, pp. 270 – 276, 2015.

[11] T. Sasaki, M. Nakajima, T. Kawamura, and K. Horioka, "Electrical conductivities of aluminum, copper, and tungsten observed by an underwater explosion," *Physics of Plasmas*, vol. 17, no. 8, p. 084501, 2010.

[12] D. Sheftman and Y. E. Krasik, "Evaluation of electrical conductivity and equations of state of non-ideal plasma through microsecond timescale underwater electrical wire explosion," *Physics of Plasmas*, vol. 18, no. 9, p. 092704, 2011.

[13] J. Stephens, J. Dickens, and A. Neuber, "Semiempirical wide-range conductivity model with exploding wire verification," *Physical Review E*, vol. 89, no. 5, p. 053102, 2014.

[14] A. Vanderburg, F. Stefani, A. Sitzman, M. Crawford, D. Surls, C. Ling, and J. McDonald, "The electrical specific action to melt of structural copper and aluminum alloys," *IEEE Transactions on Plasma Science*, vol. 42, no. 10, pp. 3167 – 3172, 2014.

[15] G. Rodríguez Prieto, L. Bilbao, and M. Milanese, "Temporal distribution of the electrical energy on an exploding wire," *Laser and Particle Beams*, vol. 34, no. 02, pp. 263–269, 06 2016. [Online]. Available: http://journals.cambridge.org/article_S0263034616000069

[16] L. Bilbao and H. Bruzzone, "Comments on "the time evolution of the resistances and inductances of the discharges in a pulsed gas laser through its current waveforms"," *IEEE Transactions on Plasma Science*, vol. 26, no. 1, pp. 119–121, Feb 1998.

[17] C. Nash and W. McMillan, "On the mechanism of exploding wires," *Physics of Fluids (1958-1988)*, vol. 4, no. 7, pp. 911–917, 1961.

[18] A. W. DeSilva and H.-J. Kunze, "Experimental study of the electrical conductivity of strongly coupled copper plasmas," *Physical Review E*, vol. 49, pp. 4448–4454, May 1994. [Online]. Available: http://link.aps.org/doi/10.1103/PhysRevE.49.4448

[19] A. Grinenko, Y. E. Krasik, S. Efimov, F. G., and V. T. Gurovich, "Nanosecond time scale, high power electrical wire explosion in water," *Physics of Plasmas*, vol. 13, no. 4, p. 042701, 2006.

[20] H. Bruzzone, H. Kelly, and C. Moreno, "On the effect of finite closure time of switches in electrical circuits with fast transient behavior," *American Journal of Physics*, vol. 57, no. 1, pp. 63 – 66, 1989. [Online]. Available: http://scitation.aip.org/content/aapt/journal/ajp/57/1/10.1119/1.15872

[21] B. E. Fridman, P. Persephonis, V. Giannetas, A. Ioannou, J. Parthenios, and C. Georgiades, "Comments on "the time evolution of the resistances and inductances of the discharges in a pulsed gas laser through its current waveforms" [with reply]," *IEEE Transactions on Plasma Science*, vol. 25, no. 4, pp. 799 – 801, Aug 1997.

[22] R. A. Matula, "Electrical resistivity of copper, gold, palladium, and silver," *Journal of Physical and Chemical Reference Data*, vol. 8, no. 4, pp. 1147 – 1298, 1979. [Online]. Available: http://scitation.aip.org/content/aip/journal/jpcrd/8/4/10.1063/1.555614

[23] L. Bilbao, "A three-dimensional finite volume arbitrary lagrangian-eulerian code for plasma simulations," *AIP Conference Proceedings*, vol. 875, no. 1, pp. 467 – 472, 2006. [Online]. Available: http://scitation.aip.org/content/aip/proceeding/aipcp/10.1063/1.2405990

ACKNOWLEDGMENT

This study has been partially supported by the Ministerio de Energía y Competitividad of Spain (ENE2013-45661-C2-1-P) and Junta de Comunidades de Castilla-la Mancha (EII-2014-008-P). Authors would like to thank Prof. Roberto Piriz for comments and suggestions.

[4] DRAFT, A SER ENVIADO

Copper metallic gas resistivity measurements by means of an explodign wire in air.

Luis Bilbao, Gonzalo Rodríguez Prieto

February 17, 2017

Abstract

Explosion of a metallic wire by means of a large electrical current has been used commonly to create metallic plasma states difficult to reach by other means. A magnitude commonly measured has been the conductivity or its inverse, the resistance, of the created plasma, due its important relation with constitutive parameters of the matter. To the knowledge of the authors of this works, such attention has not been paid to the resistivity of the metallic gas generated in the dark current pause that appears in the exploding wire when surrounded by a dense medium, like atmospheric air. In this work we present experimental limits for the copper metallic gas resitivity values as a function of the temperature. Measured limits for the resistivity of the copper gas are between 0.004 and 0.008 Ohm·m at the ionizing temperature and from 0 to 0.004 Ohm·m at the copper boiling temperature.

1 Introduction

An exploding wire consists on a thin metalic wire, typically with a diameter on the order of micrometers and centimeters length, through which a large electrical current passes, causing the transformation of the metal in liquid, gas, and finally plasma by the fast heating by Joule effect [1]. It is a phenomen known to science since a long time [2], consecuently has been used in multiple scientific investigations [3, 4, 5].

One of the phenomena that can be investigated with an exploding wire is the so called dark current pause. Shortly after the current discharge, when the wire material has become gas, its conductive capabilities are so low that the current is almost halted until furhter gas expansion allows for the plasma formation [3, 6]. The metallic gas of the dark current has not been probed extensively, on the contrary of the resistance and other carachteristics of the formed plasma. These carachteristics can be measured indirectly through the appropiate treatment of the electrical signals, voltage and current, thorough the wire. Typical examples are the experimental works [7, 8].

*L. Bilbao is with Universidad de Buenos Aires, Argentina.
†G. Rodríguez Prieto is with Universidad de Castilla-La Mancha, Spain and INEI, Ciudad Real, Spain

Among these plasma carachteristics, its conductivity has been measured experimentally in different materials and situations with an exploding wire setup [9, 10, 11, 12].

Measurement of the resisitivity of the metallic gas has not been addressed in the open literature, to the knowledge of the authors of this work. Here we present the first measurements for the limits of metallic gas conductivity for the Copper metal. Simulations performed on the voltage and current in the wire with the obtained metallic gas resistivity show an excellent agreement with experimental data.

2 Experiment and physical model description

Experiments were performed with the ALEX (*ALambre EXplosivo*, exploding wire in Spanish) system, shown schematically in Fig. 1. ALEX is formed by two capacitors in parallel, 1.1 μF each, connected to a high voltage source, maximum charging voltage 60 kV, which discharges the capacitors through a metallic wire surrounded by atmospheric air when the spark gap is closed by a high voltage trigger pulse.

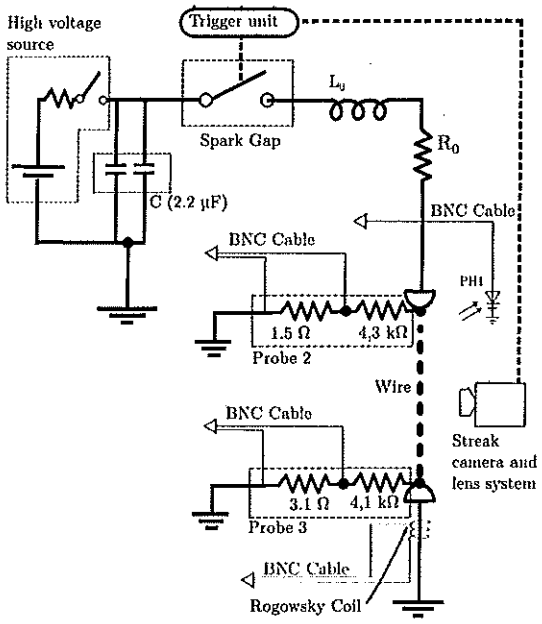

Figure 1: Exploding wire setup. PH1 signals the photodiode, C the capacitors bank, and L_0 and R_0 the lumped inductance and resistance of the setup, respectively.

The high voltage trigger pulse is synchronized with the streak camera unit by the depicted trigger unit. In order to perform the measurements of the metallic gas resistivity limits here described, it is necessary to know the radial expansion of the metallic gas. In this work radial expansion was obtained from direct shadowgraphy images recorded with the streak unit for each experiment.

Voltages from the probes 2 and 3 and the Rógowsky coil signals, along with the photodiode signal, were also recorded in an oscilloscope enclosed in a Faraday cage room. The photodiode signal was used to synchronize the streak camera photos with the electrical signals with a precision of $\pm$ 60 ns.

Copper wires with fixed length of 5.1 cm and diameter of 50 μm were used in these experiments. Different charging voltages, 10, 15, 18, 21 and 25 kV were employed to assure that the measured resistivity limits were consistent with different initial energies and therefore, with the dinamical behaviour of the metallic wire associated with the initial energy [5].

In order to calculate the voltage across the wire, some calculations over the obtained voltages from probe 2 and 3 are necessary. Using a path along the wire boundary, as Fig. 2 shows, the circuit equation reads

$$\frac{d\Phi_b}{dt} + \int_b \mathbf{E}' \cdot d\mathbf{l} = \frac{Q}{C} - R_0 I - L_0 \frac{dI}{dt} - V_{sg}(t), \tag{1}$$

where Φ_b is the magnetic flux enclosed by the circuit formed by the path b, $\mathbf{E}'$ the electric field in a system fixed to the path $d\mathbf{l}$, C the capacitance of the capacitor bank, R_0 and L_0 the lumped resistance and inductance of the circuit, V_{sg} the voltage drop across the spark gap, I the current, and Q the charge.

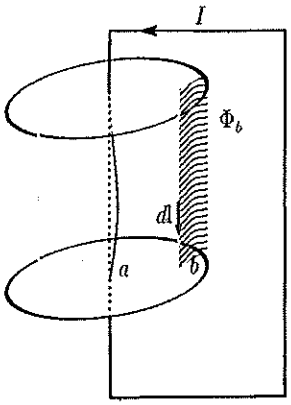

Figure 2: Exploding wire path to calculate the circuit equation.

Therefore, the voltage across the wire, V_{wire}, can be written as:

$$V_{wire} = \frac{d\Phi_b}{dt} + \int_b \mathbf{E}' \cdot d\mathbf{l}. \tag{2}$$

Since the flux, Φ_b, is calculated beyond the border of the wire, and due to the fact that there is no electrical current circulating in the surrounding atmospheric air, the flux variation in time can be written as

$$\frac{d\Phi_b}{dt} = \frac{d(L_b I)}{dt}, \tag{3}$$

where L_b is a geometrical function equivalent to the inductance calculated between the boundary of the wire and the returning conductor. In our case, the

returning conductor is a plane plate at a fixed distance d from the wire center, thus considering atmospheric air as the medium, we get

$$L_b = \frac{\mu_0 l}{2\pi} \cosh^{-1}\left(\frac{d}{r_b}\right), \tag{4}$$

being l the length of the wire and r_b its radius (that varies with time).

On the other hand, using the Ohm law in a system fixed to the wire, the second term on the right hand side of (2) is :

$$\int_b \mathbf{E}' \cdot d\mathbf{l} = \int_b \rho \mathbf{j} \cdot d\mathbf{l}, \tag{5}$$

where ρ is the resistivity and $\mathbf{j}$ the current density.

Note that the integration of $\mathbf{j}$ across a section, $d\mathbf{S}$, of the wire gives the total current:

$$\int \mathbf{j} \cdot d\mathbf{S} = \mathrm{I}. \tag{6}$$

Finally, substituting in ec. (2) the values given by ecs. (3) and (5) we get

$$V_{wire} = \frac{d(L_b I)}{dt} + \int_b \rho \mathbf{j} \cdot d\mathbf{l}. \tag{7}$$

In case of cylindrical symmetry the above reduces to

$$V_{wire} = \frac{d(L_b I)}{dt} + l(\rho j_z)_b, \tag{8}$$

being z the direction of the axis of the cylinder, with the subscript b indicating that the variables are calculated on the wire boundary.

The voltage across the wire is measured by means of the two voltage dividers mentioned, as shown in Fig.1. The probe 2 measures the voltage drop, V_2, that includes part of the anode, the wire, the cathode, and the returning path to ground. Instead, probe 3 measures the voltage drop, V_3, that only includes the cathode and the returning path to ground. Therefore, the measured voltage, V_{meas}, is

$$V_{meas} \equiv V_2 - V_3 = V_{wire} + V_{anode}, \tag{9}$$

where V_{anode} is the voltage drop in the part of the anode included in probe 2.

This contribution can be modeled by a lumped element model, that is

$$V_{anode} = L_{anode}\frac{dI}{dt} + R_{anode} I. \tag{10}$$

The current derivative dI/dt is measured with the Rogowski coil, and its numerical integration gives the current I.

Parameters L_{anode} and R_{anode} can be obtained by two different methods. When $V_{ew} << V_{anode}$ (as expected in the final part of the discharge, when a plasma is formed), the voltage (9) can be approximatated by a multilinear linear approximation of the electrical current and its derivative. Or on a simpler way, by removing the wire and joining the electrodes, as it was done during the Rogowsky coil calibration procedure, thus forcing a shot circuit in the electrical system. In both cases the measured voltage is

$$V_{shortcircuit} = L_{anode}\frac{dI}{dt} + R_{anode} I,$$

and therefore the parameters L_{anode} and R_{anode} are obtained using a multiple linear regression analysis of the dependent variable $V_{shortcircuit}$ and the independent variables I and $\frac{dI}{dt}$.

Once the lumped parameters of the anode are known, the voltage drop across the wire is obtained from the measurements of voltage, current, and its derivative as

$$V_{wire} = V_{meas} - L_{anode}\frac{dI}{dt} - R_{anode}I. \tag{11}$$

Using (7) in (11) we finally obtain

$$V_{res} \equiv \int_b \rho \mathbf{j} \cdot d\mathbf{l} = V_{meas} - L_{anode}\frac{dI}{dt} - R_{anode}I - \frac{d\left(L_b I\right)}{dt}. \tag{12}$$

3 Resistivity limit values and conclusions

When diffusion of the current is the dominating phenomenon inside the wire, from the Faraday's law of induction it follows that

$$\frac{d\Phi_a}{dt} + \int_a \rho \mathbf{j} \cdot d\mathbf{l} = \frac{d\Phi_b}{dt} + \int_b \rho \mathbf{j} \cdot d\mathbf{l}. \tag{13}$$

where a indicates any other path inside the wire (an Ohm's law was assumed for the wire). This means, for example, that the ohmic voltage drop depends on the path (second term on both sides of the above equation) making impossible to meaningfully define separately a resistance and an inductance of the wire as lumped parameters in the circuit under these conditions [13].

In the case in which the variation of the magnetic flux variation inside the wire, $\Phi_b - \Phi_a$, is negligible (usually expected in time scale larger than the diffusion time or, equally, skin depth values larger than the wire diameter), that is

$$\frac{d\left(\Phi_b - \Phi_a\right)}{dt} \approx 0, \tag{14}$$

the ohmic voltage drop becomes independent of the path

$$\int_a \rho \mathbf{j} \cdot d\mathbf{l} = \int_b \rho \mathbf{j} \cdot d\mathbf{l}, \tag{15}$$

and a resistance variable in time can be defined as

$$R = \frac{\int_b \rho \mathbf{j} \cdot d\mathbf{l}}{I}. \tag{16}$$

Such is the case of the experiments here presented, as the skin depth value for copper at the circuit frequency is on the order of 120 μm, more than three times the wire diameter.

According to (7), the resistance above can experimentally be obtained from the electrical signals as

$$R = \frac{V_{res}}{I} = \frac{V_{meas} - L_{anode}\frac{dI}{dt} - R_{anode}I - \frac{d(L_b I)}{dt}}{I}, \tag{17}$$

where the "border inductance" L_b is evaluated using (4) from the measurement of the evolution of the wire boundary radius, r_b.

Although the resistance R may experimentally be obtained, it is not simple to calculate the resistivity of the wire from it, unless the current density is known. Unfortunately there are no simple probes that are able to measure the current density inside sub-millimeter wires. Therefore, we will discuss what valuable information can be extracted when the electrical current density distribution is unknown.

As it was mentioned above, when the magnetic flux variation inside the wire is important (i.e. during the diffusion period) the value from (17) is not only a resistive term. Thus, in order to use (17) care should be taken in identifying the period of time where the magnetic flux variation inside the wire is negligible.

In case of negligible magnetic flux variation inside the wire, assuming cylindrical symmetry (that will be used in what follows), from (16), the calculation of a mean resistivity from the measured resistance (17) gives

$$\langle \rho \rangle = \frac{RS}{l}, \tag{18}$$

where S is the section of the wire.

The value from (18) will represent the resistivity of the wire as long as a relatively uniform resistivity is expected. This is not the case during the dark pause where different states may coexist. In fact, numerical simulations show the presence of a liquid inner core surrounded by a gaseous outer layer, and as there are many orders of magnitude between the resistivity of a metallic gas and that of a metallic liquid, the obtention of the mean value from ec. 18 is useless.

Independently of this fact, from (15) we get

$$\rho j_z = const, \tag{19}$$

where the constant in space varies with time. Evaluating the constant at the boundary, the variation of the current density along the radius depends on the resistivity as

$$j_z = \frac{(\rho j_z)_b}{\rho}, \tag{20}$$

that using (16) becomes

$$j_z = \frac{RI}{\rho l}. \tag{21}$$

Integrating on cross section we get :

$$I = \int 2\pi r j_z dr = \frac{RI}{l} \int \frac{2\pi r dr}{\rho}, \tag{22}$$

or

$$\frac{1}{R} = \frac{2\pi}{l} \int \frac{r dr}{\rho}. \tag{23}$$

Assuming that there is an inner liquid region and an outer gaseous region, each one with relatively uniform resistivity, the above becomes

$$\frac{1}{R} = \frac{2\pi}{l} \int_{liquid} \frac{r dr}{\rho} + \frac{2\pi}{l} \int_{gas} \frac{r dr}{,} \rho \tag{24}$$

or

$$\frac{1}{R} = \frac{S_{liquid}}{l \langle \rho \rangle_{liquid}} + \frac{S_{gas}}{l \langle \rho \rangle_{gas}}, \tag{25}$$

where S_{liquid} is the section of the inner core, S_{gas} the section of the outer core, and $\langle\rho\rangle_{liquid/gas}$ represents a mean value on each phase.

Defining the resistance for each state as:

$$R_{liquid} = \frac{l\,\langle\rho\rangle_{liquid}}{S_{liquid}}, \quad \text{and} \quad R_{gas} = \frac{l\,\langle\rho\rangle_{gas}}{S_{gas}}, \tag{26}$$

we finally get

$$\frac{1}{R} = \frac{1}{R_{liquid}} + \frac{1}{R_{gas}}. \tag{27}$$

The total resistance of the wire corresponds to a parallel of the resistance of the liquid and the gas phase, as expected.

From the electrical signals it is not possible to determine the relative contribution of each state to the total resistance. Anyway, the total resistivity represents a limit to each individual resistance :

$$R < R_{liquid}, \quad \text{and} \quad R < R_{gas}, \tag{28}$$

from which resistivity limits can be measured as

$$\langle\rho\rangle_{liquid} > \frac{RS_{liquid}}{l}, \tag{29}$$

for the liquid and

$$\langle\rho\rangle_{gas} > \frac{RS_{gas}}{l}, \tag{30}$$

in the case of the metallic gas.

Note that as the gas expands much more than the liquid and therefore, its surface is much larger than the one of the liquid,the section of the gas can be taken as the total section of the expanded wire, that is

$$S_{gas} \approx \pi r_b^2. \tag{31}$$

By measuring the dependence of the boundary radius, r_b, with time and the electrical signals leading to the resistive voltage measurements, a lower bound of the mean gas resistivity is given as

$$\langle\rho\rangle_{gas} > \frac{R\pi r_b^2}{l} = \frac{V_{res}\pi r_b^2}{lI}, \tag{32}$$

where R is obtained from (17).

In principle, a similar procedure may be used for obtaining a lower bound for the resistivity of the metallic liquid. The problem is that, from the measurements, there is no simple way to determine the physical limit between liquid and gas phases, therefore the section of this region, S_{liquid}, cannot be estimated.

In order to estimate the lower limit for the gas resitivity, it is necesassary to consider the energy transfer from the electrical circuit to the exploding wire during the dark pause. The dark pause starts when the metallic gas is formed in the outer layer, and it lasts until the ionization of the plasma begins. Due to the large resistivity of the gas, the dark pause is characterized by a low current, a fact that is easily seen in the electrical signals. Therefore, during the dark

pause, the metallic gas is heated from the boiling point to the ionizing point by Joule heating. The power for the Joule heating of the gas is

$$\dot{W}_j = \int_{gas} \rho \mathrm{j}^2 dV, \tag{33}$$

that, using cylindrical symmetry and (19), can be rewritten as

$$\dot{W}_j = (\rho j_z)^2 \int_{gas} \frac{1}{\rho} dV, \tag{34}$$

or, in virtue of (26)

$$\dot{W}_j = l\,(\rho j_z)^2 \int \frac{2\pi r}{\rho} dr = \frac{(l\rho j_z)^2}{R_{gas}} = \frac{V_{res}^2}{R_{gas}}. \tag{35}$$

As a matter of fact, from the experiments we find that $V_{res} \approx const$ during the dark pause, excepted for a few hundred of nanoseconds at the beginning of the discharge.On the other hand, the gas resistivity is observed to decrease with time, mainly due to the expansion of the gas.

The energy delivered to the gas up to a given time t should be enough to heat up the gas to the temperature at that time instant. Therefore, integrating the power in time from the beginning up to a given time instant t, that is

$$\frac{V_{res}^2}{\langle R \rangle_{gas}} (t - t_{boiling}) \geq n\,(t)\, C_p\, (T - T_{boiling}), \tag{36}$$

where T is the gas temperature at time t, $n\,(t)$ the number of moles in the gas state, C_p the molar heat capacity at constant pressure, $T_{boiling}$ the boiling temperature, and $\langle R \rangle_{gas}$ a mean value of the resistance of the gas.

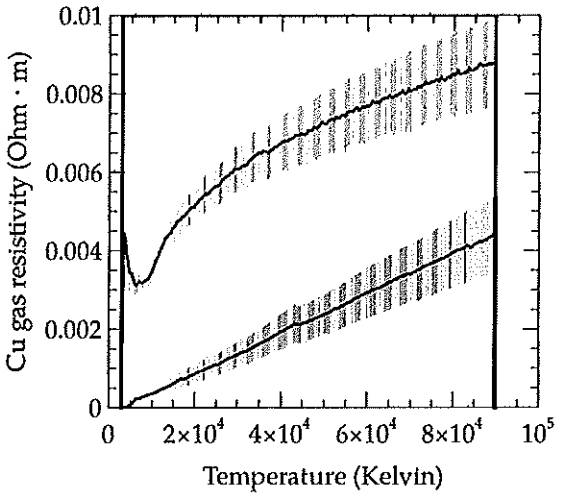

Figure 3: Copper gas resistivity experimental limits. Shadows correspond to the experimental error bars.

A first approach solution for the temperature is obtained assuming the same linear dependence with time of both, number of moles and temperature:

$$\frac{T - T_{boiling}}{T_{ionizing} - T_{boiling}} = \frac{t - t_{boiling}}{t_{ionizing} - t_{boiling}} = \frac{n(t)}{n}, \tag{37}$$

where $T_{ionizing}$ is the ionizing temperature, and n the total number of moles (i.e., the entire wire is in gas state at the end of the dark pause). Thus (36) becomes

$$\frac{V_{res}^2}{\langle R \rangle_{gas}} (t_{ionizing} - t_{boiling}) \geq nC_p (T_{ionizing} - T_{boiling}) \frac{t - t_{boiling}}{t_{ionizing} - t_{boiling}}, \tag{38}$$

and finally for the mean gas resistance

$$\langle R \rangle_{gas} \leq \frac{V_{res}^2 (t_{ionizing} - t_{boiling})^2}{nC_p (T_{ionizing} - T_{boiling}) (t - t_{boiling})}, \tag{39}$$

or for the resistivity

$$\langle \rho \rangle_{gas} \leq \frac{r_b^2 V_{res}^2 (t_{ionizing} - t_{boiling})^2}{nC_p l (T_{ionizing} - T_{boiling}) (t - t_{boiling})}. \tag{40}$$

Note that (40) should be taken with care during the initial stage, when diffusion is important and (19) is not valid.

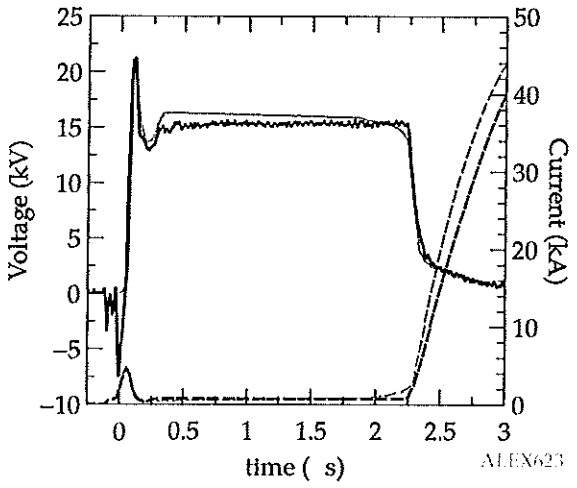

Figure 4: Wire voltage (cont. lines) and current (dashed lines) signals for a charging voltage of 18 kV. Black lines indicate the experimental values and grey lines the calculated ones.

The time duration of the dark pause depends on our experiments only of the initial voltage. Therefore, the time scale needs to be rescaled in order to compare different experimental measurements at different voltages. The way here employed is the replacement of time by temperature using (37).

In figure 3 the mean values of the two previously deduced limits, (32) and (40), are plotted as a function of temperature. The electrical signals were obtained from the electrical probes (as described above), while the evolution of the radius was taken from the streak camera images.

In order to check the hypothesis and values of the limits of the resistivity here presented, the experiment was simulated using a simplified, 1D version of a full 3D multi-component (neutrals, ions, and electrons), two temperature, Arbitrary Lagrangian-Eulerian, Finite Volume code [14]. The coupling with the exploding wire experiment is described in [15]. Browsing different values for the resistivity within the above limits, we get a fairly good reproduction of the electrical behavior using

$$\rho = \rho_0 \ (1 + \alpha\,(T - T_{boiling})) \tag{41}$$

with $\rho_0 = 0.00004\ \Omega{\cdot}\mathrm{m}$ and $\alpha = 0.00186/\mathrm{K}$.

With this resistivity function, many features of the electrical signals are reproduced. As figure 4 shows, calculated and experimental values of the initial peak of the voltage are in very good agreement. Time length of the dark pause, marked both by the voltage and current plateau and the slope of rise up (down) of the current(voltage) at the end of the dark pause, is also very well reproduced by the calculations with the above function for the copper gas resistivity. Similar observations can be made about the values of the radial border of the plasma expansion, as Fig. 5 shows.

Despite the good agreement between the calculated values and the experimental ones using the resistivity limits as guide, there is room for improvement as there are still non modeled features. For example, the initial negative voltage peak observed in the experiments is not reproduced by the simulations. Also, the transition from liquid to gas, i.e. the liquid-gas state, needs to be modeled. On the other hand, in the simulations, a linear dependence of the resistivity with the enthalpy has been used.

We are aware of the speculative character of many hypothesis, but the aim of this notes is to set limits for the electrical conductivity of copper gas, that to the best of our knowledge, have never been measured. Improvements may be performed in the experiments and the numerical simulations in order to determine a more precise value. For example, we have used a oscilloscope with only 8-bit vertical resolution. This produces a large indetermination of the current during the dark pause, because the scale is set in order to capture the peak current, that is much larger than the current during the dark pause.

4 References

References

[1] F. D. Bennett, R. Hefferlin, and R. A. Strehlow, *Progress in high temperature physics and Chemistry. Volume II.* High-temperature exploding wires, Pergamon Press, London, 1969.

[2] E. Nairne, "An account of the effect of electricity in shortening wires," *Philosophical Transactions of the Royal Society of London*, vol. 70, pp. 334 – 337, 1780.

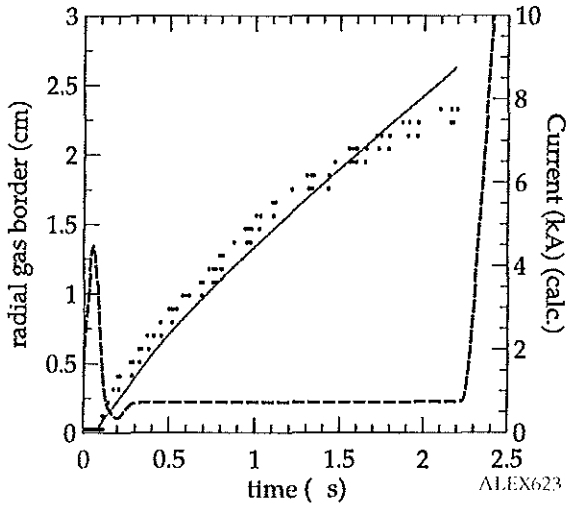

Figure 5: Radial expansion of the metallic gas (points, experimental values, grey line calculated) and calculated current values (dashed line). Notice the low values in the current scale.

[3] C. P. Nash and W. G. McMillan, "On the mechanism of exploding wires," *Physics of Fluids*, vol. 4, pp. 911 – 917, 1961.

[4] S. V. Lebedev and S. A. Savvatimskii, "Metals during rapid heating by dense currents," *Soviet Physics Uspekhi*, vol. 27, no. 10, pp. 749 – 771, 1984.

[5] D. B. Sinars, M. Hu, K. M. Chandler, T. A. Shelkovenko, S. A. Pikuz, J. B. Greenly, D. A. Hammer, and B. R. Kusse, "Experiments measuring the initial energy deposition, expansion rates and morphology of exploding wires with about 1 ka\wire," *Physics of Plasmas*, vol. 8, no. 1, pp. 216 – 230, 2001.

[6] K. M. Chandler, D. A. Hammer, D. B. Sinars, S. A. Pikuz, and T. A. Shelkovenko, "The relationship between exploding wire expansion rates and wire material properties near the boiling temperature," *IEEE Transactions on Plasma Science*, vol. 30, no. 2, pp. 577 – 587, 2002.

[7] F. D. Bennett, "Initial heating rates and energy inputs for exploding wires," *Physics of fluids*, vol. 7, pp. 147 – 148, 1964.

[8] P. U. Duselis and B. R. Kusse, "Experimental observation of plasma formation and current transfer in fine wire expansion experiments," *Physics of Plasmas*, vol. 10, no. 3, pp. 565 – 568, 2003.

[9] A. W. DeSilva and J. D. Katsouros, "Electrical conductivity of dense copper and aluminum plasmas," *Physical Review E*, vol. 57, no. 5, pp. 5945 – 5951, 1998.

[10] S. I. Tkachenko, V. M. Romanova, A. R. Mingaleev, A. E. Ter-Oganesyan, T. A. Shelkovenko, and S. A. Pikuz, "Study of plasma's parameter distribution upon electrical wire explosion," *The European Physical Journal D*, vol. 54, no. 2, pp. 335 – 341, 2009.

[11] T. Sasaki, M. Nakajima, T. Kawamura, and K. Horioka, "Electrical conductivities of aluminum, copper, and tungsten observed by an underwater explosion," *Physics of Plasmas*, vol. 17, no. 8, p. 084501, 2010.

[12] D. Sheftman and Y. E. Krasik, "Investigation of electrical conductivity and equations of state of non-ideal plasma through underwater electrical wire explosion," *Physics of Plasmas*, vol. 17, no. 11, p. 112702, 2010.

[13] L. Bilbao, H. Bruzzone, P. Persephonis, V. Giannetas, A. Ioannou, J. Parthenios, and C. Georgiades, "Comments on "the time evolution of the resistances and inductances of the discharges in a pulsed gas laser through its current waveforms" [with reply]," *IEEE Transactions on Plasma Science*, vol. 26, pp. 119–121, Feb 1998.

[14] L. Bilbao, "A threedimensional finite volume arbitrary lagrangianeulerian code for plasma simulations," *AIP Conference Proceedings*, vol. 875, no. 1, pp. 467–472, 2006.

[15] G. Rodríguez Prieto, L. Bilbao, and M. Milanese, "Temporal distribution of the electrical energy on an exploding wire," *Laser and Particle Beams*, vol. 34, pp. 263–269, 06 2016.

[5]

Does the Velocity of Light Depend on the Source Movement?

Luis Bilbao
Universidad de Buenos Aires. Consejo Nacional de Investigaciones Científicas y Técnicas.
Instituto de Física del Plasma (INFIP). Facultad de Ciencias Exactas y Naturales. Buenos Aires, Argentina.
E-mail: bilbao@df.uba.ar

Data from spacecrafts tracking exhibit many anomalies that suggest the dependence of the speed of electromagnetic radiation with the motion of its source. This dependence is different from that predicted from emission theories that long ago have been demonstrated to be wrong. By relating the velocity of light and the corresponding Doppler effect with the velocity of the source at the time of detection, instead of the time of emission, it is possible to explain quantitatively and qualitatively the spacecraft anomalies. Also, a formulation of electromagnetism compatible with this conception is possible (and also compatible with the known electromagnetic phenomena). Under this theory the influence of the velocity of the source in the speed of light is somewhat subtle in many practical situations and probably went unnoticed (i.e. below the detection limit) in other measurements.

1 Introduction

In these lines I intend to show that there exists consistent evidence pointing to the need of revision and further study of what seem at present a settled issue, namely the independence of the speed of electromagnetic radiation on the motion of its source.

The main point in the evidence is the range disagreement during the Earth flyby of the spacecraft NEAR in 1998. Its range was measured near the point of closest approach using two radar stations, Millstone and Altair, of the Space Surveillance Network, and compared with the trajectory obtained from the Deep Space Network [1]. As for the range, the two measurements should match within a meter-level accuracy (the resolution is 5 m for Millstone and 25 m for Altair), but actual data showed a difference that varies linearly with time (with different slopes for the two radar stations) up to a maximum difference of about 1 km, i.e. more than 100 times larger than the accuracy of the equipment used (see figure 10 of [1]). Further, when NEAR crossed the orbits of Global Positioning System (GPS) satellites, orbital radius 26,600 km, the measured range difference was 650 m, that is, a time difference of 2 μs. Is it reasonable that any standard GPS receiver performs better than the Deep Space Network or the Space Surveillance Network?

There has not been a complete explanation for the range discrepancy. It is very difficult to find any physical reason that may produce this anomaly, for any physical disturbance of the path of the spacecraft should manifest equally in the Deep Space Network and the Space Surveillance Network data. Guruprasad [2] proposed an explanation that points to a time lag in the Deep Space Network signals proportional to the range, but the model is, at best, within 10% of the measured data (i.e. larger than the instrumental error) and, more important, it fails to explain an important feature, that is, the different slope for the two radars. If we assume that systems are working properly, then the measured range difference (time lag) could be due to different propagation time of the employed signals.

Additional points in the evidence come from anomalies related to the tracking of spacecrafts, present in both Doppler and ranging data. The Pioneer anomaly [3] and the flyby anomaly [4] refer to small residuals of the differences between measured and modeled Doppler frequencies of the radio signals emitted by the spacecrafts. Although these residuals are very small (less than 1 Hz on GHz signals) the problem is that they follow a non-random pattern, indicating failures of the model. According to the temporal variation of those residuals the Pioneer anomaly exhibits a main term, an annual term, a diurnal term and a term that appears during planetary encounters. It should be clarified that a few years ago an explanation of the Pioneer anomaly was published [5]. However, it is a very specific solution that applies only to the main term of the Pioneer spacecraft anomaly, but left unresolved many other anomalies, including those of the spaceships Cassini, Ulysses and Galileo; the annual term; the diurnal term; the increases of the anomaly during planetary encounters; the flyby anomaly; and the possible link between all them (it is hard to think that there are so many different causes for the mentioned anomalies). For all this, I believe that the issue can not be closed as it stands.

2 Range disagreement

As a matter of fact, the range difference between the Space Surveillance Network and the Deep Space Network, δR, is perfectly fitted with

$$\delta R(t) = -\frac{\mathbf{R}(t)\cdot\mathbf{v}(t)}{c}, \qquad (1)$$

where $\mathbf{R}(t)$ is a vector range pointing from the spacecraft to the radar, $\mathbf{v}(t)$ the spacecraft velocity relative to the radar,

and c the speed of light. Figure 1 shows this fit and its comparison with measured data. The orbital and measured data were taken from [1]. Although the exact location of the radar stations are unknown to the author (approximate values are: Millstone 42.6° N 71.43° W, and Altair 9.18° N 167.42° E), the fit is statistically significant for both radar stations ($p < 10^{-3}$) including the first outliers points. It reproduces the (almost) linear dependence with time during the measured interval, and the two different slopes for Millstone and Altair stations due to their different locations.

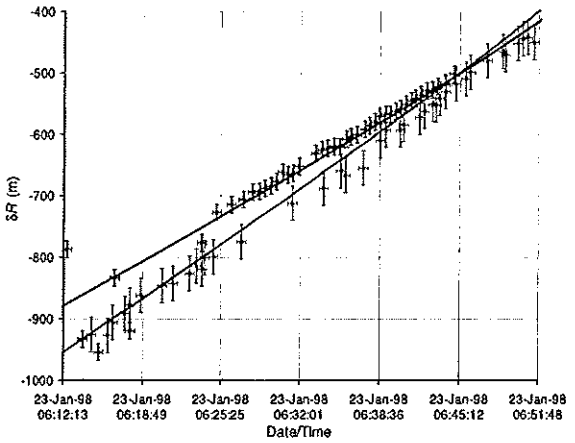

Fig. 1: Range disagreement between the Space Surveillance Network and the Deep Space Network, for 1998 NEAR flyby (Millstone blue points, upper trace, and Altair red points, lower trace). Also the fit (1) is plotted (full lines, Millstone in blue and Altair in red). For Millstone, the error bars refer to the uncertainties in the extraction of the data from figure 10 of [1], rather than to its tracking error (5 m), while for Altair, the accuracy is 25 m.

Since range measurements are based on time-of-flight techniques, the validity of (1) means that the electromagnetic waves (microwave) of the Deep Space Network and the Space Surveillance Network travel at different speeds. Specifically, in the radar frame of reference, if the Space Surveillance Network waves travel at c, then the Deep Space Network waves travel at c plus the projection of the spacecraft velocity in the direction of the beam, in sharp contrast with the Second Postulate of the Special Relativity Theory.

In view of the above result one may ask what is established, at present, about the relation of the speed of electromagnetic radiation (light for short) to the motion of the source. In order to elaborate this point the following questions are of relevance:

1. Are there *simultaneous* measurements of the speed of light from different moving macroscopic sources (not moving images) with different velocities?;
2. Since ballistic (emission) theories are ruled out (see, for example, DeSitter [6, 7], Brecher [8] and Alväger et al [9]), how else could the speed of light depend on the source movement?;
3. How is it possible that there is a first order difference in v/c in spacecraft range measurements, while at the same time there are many experiments on time dilation that are consistent with Special Relativity Theory to second order in v/c (see, for example, [10])?;
4. If the velocity of light depend on the velocity of the source, why has this not been observed in other phenomena in the past?

In answer to the previous questions, so far as the author is aware, there is no known experimental work that simultaneously measures the speed of light from two different sources (not images), or that simultaneously measures the speed of light and that of its source. For example, in the work by Alväger et al, [9] the speed of light is measured at a later time ($\approx$ 200 ns) than the emission time, and there is no measurement of the speed of the source at the time of the *detection* of the light.

Note that measurements involving moving images produce different results from those produced by mobile sources. For example, under Special Relativity Theory, a moving source is affected by time dilation while a moving image is not. Therefore, to ensure the independence of the speed of light from its source movement, it is essential to have two sources with different movements.

Although controversial and beyond the scope of the this note, time dilatation phenomena may be of different physical origin from first order terms, as it may be inferred from the work of Schrödinger [11]. Thus, measurements of time dilatation phenomena in accordance with Special Relativity Theory, does not necessarily imply the independence of the speed of light with the movement of the source.

The experiments mentioned above [6–9] only rule out ballistic theories in which radiation maintains the speed of the source at the time of *emission*, but do not rule out other ideas, like Faraday's 1846 [12].

3 Faraday's ray vibrations

In order to remove the ether, Faraday introduced the concept of vibrating rays [12], in which an electric charge is conceived as a center of force with attached "rays" that extend to infinity. The rays move with their center, but without rotating. According to this view, the phenomenon of electromagnetic radiation corresponds to the vibration of these "rays", that propagates at speed c relative to the rays (and the center). That is, the radiation remains linked to the source even after emitted. Today we could describe the interaction as a kind of entanglement between the charge and the photon. A framework for the electromagnetic phenomena according to Faraday's ideas was developed. It was called "Vibrating Rays Theory" [13] in reference to Faraday's "vibrating rays".

Under Faraday's idea, the velocity of radiation at a given epoch will be equal to c plus the velocity of the source at the *same* epoch, in contrast with ballistic theories in which

the emitted light retains the speed of the source at the *emission* epoch. In this sense the radiation is always linked to the charge at every time after the emission. Consequently, the measured Doppler Effect corresponds to the speed of the source at the time of *reception*, as well.

Further, a difference between active and passive reflection is expected, since the latter is still related to the original source according to Vibrating Rays Theory. The Deep Space Network works with the so called active reflection (the spacecraft re-emits in real time a signal in phase with the received signal from Earth), while the Space Surveillance Network works with passive radar reflection. In consequence, the down-link signal from the approaching spacecraft will propagate faster that the reflected one. Using the available orbital data [1] we found that, under Vibrating Rays Theory, the theoretical time-of-flight difference between active and passive reflection gives exactly the same range disagreement as (1), see Part 6 of [13].

4 Pioneer anomaly

The Pioneer anomaly refers to the fact that the received Doppler frequency differs from the modeled one by a blue shift that varies almost linearly with time, and whose derivative is

$$\frac{d(\Delta f)}{dt} \approx -6 \times 10^{-9}\ \text{Hz/s}, \tag{2}$$

where Δf is the frequency difference between the measured and the modeled values.

In the case of a source with variable speed, the main difference in Doppler (to first order) between Vibrating Rays Theory and Special Relativity Theory, is that Special Relativity Theory relates to the speed of the source at the time of *emission*, while Vibrating Rays Theory relates to the speed of the source at the time of *reception*. Precisely, this difference seems to be present in the spacecraft anomalies.

If Vibrating Rays Theory is valid, it automatically invalidates all calculations and data analysis of spacecraft tracking which are based on Special Relativity Theory. So, it is not easy to make a direct comparison between the expected results from Special Relativity Theory and Vibrating Rays Theory. However, to see whether or not the main features predicted by Vibrating Rays Theory are present in the measurements, we can evaluate the residual by simulating a measured Doppler signal assuming that light propagates in accordance to Vibrating Rays Theory but analyzed according to Special Relativity Theory.

Calling t_2 the emission time of the downlink signal from the spacecraft toward Earth and t_3 the reception time at Earth, the first order difference of the Doppler shift between Vibrating Rays Theory and Special Relativity Theory is (see [13] Part 4)

$$\Delta f = f_{VRT} - f_{SRT} \approx f_0 \hat{\mathbf{r}} \cdot \frac{\mathbf{v}_2 - \mathbf{v}_3}{c}, \tag{3}$$

where $\mathbf{v}_2$ and $\mathbf{v}_3$ represent the velocities of the spacecraft at the corresponding epoch, $\hat{\mathbf{r}}$ is the unit vector from the spaceship to the antenna, and f_0 the proper frequency of the signal. That is, the velocity used in the Special Relativity Theory formula is that at the time of *emission* while according to Vibrating Rays Theory is that corresponding at the time of *reception*.

Since the spacecraft slows down as it moves away, then $\hat{\mathbf{r}} \cdot (\mathbf{v}_2 - \mathbf{v}_3) > 0$, therefore the difference corresponds to a small blue shift mounted over the large red shift, as it has been observed in the Pioneer anomaly. It should be noted that this difference appears because of the active reflection produced by the on-board transmitter. In case of a passive reflection (for example, by means of a mirror) the above difference vanishes.

4.1 Main term

An estimate of the order of magnitude of 3 is obtained by using that the variation of the velocity of the spacecraft between the time of emission and reception is approximately

$$\mathbf{v}_2 - \mathbf{v}_3 \approx \mathbf{a}\,(t_2 - t_3), \tag{4}$$

where $\mathbf{a}$ is a mean acceleration during the down-link interval. An estimate for the duration of the down-link is simply

$$t_3 - t_2 \approx \frac{r}{c}, \tag{5}$$

where r is a mean position of the spaceship between t_2 and t_3, therefore

$$\Delta f \approx -f_0 \frac{\mathbf{r} \cdot \mathbf{a}}{c^2}.$$

Since

$$\mathbf{a} = -\frac{GM}{r^2}\hat{\mathbf{r}},$$

where G is the gravitational constant, and M the mass of the Sun, then, the time derivative becomes

$$\frac{d(\Delta f)}{dt} \approx f_0 \frac{\mathbf{v} \cdot \mathbf{a}}{c^2}. \tag{6}$$

If the difference (6) is interpreted as an anomalous acceleration we get

$$a_a \approx \frac{v}{c} a, \tag{7}$$

that is, the so-called anomalous acceleration is v/c times the actual acceleration of the spacecraft.

Using data from HORIZONS Web-Interface [14] for the spacecraft ephemeris, some characteristic value for a_a can be obtained. Consider the anomalous acceleration detected at the shortest distance of the Cassini spacecraft during solar conjunction in June, 2002. The spacecraft was at a distance of 7.42 AU moving at a speed of 5.76 km/s. The anomalous acceleration given by (7) is $a_a \approx 2 \times 10^{-9}$ m/s^2 of the same order of the measured one ($\approx 2.7 \times 10^{-9}$ m/s^2). Also, the closest distance at which the Pioneer anomaly has been detected was

about 20 AU. the anomalous acceleration predicted by (7) at that distance is $a_a \approx 7.3 \times 10^{-10}$ m/s^2 of the same order as the measured one.

The "anomaly" given by (7) decreases in time in a way that has not been observed. Note, however, that according to Markwardt [15] the expected frequency at the receiver includes an additional Doppler effect caused by small effective path length changes, given by

$$\Delta f_{path} = -\frac{2f_0}{c}\frac{dl}{dt}, \tag{8}$$

where dl/dt is the rate of change of effective photon trajectory path length along the line of sight. This is a first order effect that can partially hide the difference between Special Relativity Theory and Vibrating Rays Theory. Therefore, a more careful analysis should take into account the additional contribution of (8) in (7).

Further, other first order effects may appear, for example, by a slight rotation of the orbital plane. Due to spacecraft maneuvers or random perturbations the orbital parameters are obtained by periodically fitting the measurements with theoretical orbits. Therefore there is no straightforward way to weight the importance of these fittings in (7). In other words, data acquisition and analysis may hide part of the Vibrating Rays Theory signature.

4.2 Annual term

Apart from the residual referred to in the preceding paragraph there is also an annual term. According to Anderson et al [16] the problem is due to modeling errors of the parameters that determine the spacecraft orientation with respect to the reference system. Anyway, Levy et al [17] claim that errors such as errors in the Earth ephemeris, the orientation of the Earth spin axis or the stations coordinates are strongly constrained by other observational methods and it seems difficult to modify them sufficiently to explain the periodic anomaly.

The advantage of studying the annual term over the main term, is that the former is less sensitive to the first order correction mentioned above, and, for the case of Pioneer, also to the thermal propulsion correction [5]. Clearly, the Earth orbital position does not modify those terms.

As before, the annual term is explained by the difference between the velocity of the spacecraft at the time of emission and that at the moment of detection, which depends on whether the spaceship is in opposition or in conjunction relative to the Sun. When the spacecraft is in conjunction, light takes longer to get back to Earth than in opposition. The time difference between emission and reception will be increased by the time the light takes in crossing the Earth orbit. Specifically, taking into account the delay due to the position of Earth in its orbit, in opposition equation (5) should be written as

$$t_3 - t_2 \approx \frac{r + R_{orb}}{c}, \tag{9}$$

while in conjunction it would be

$$t_3 - t_2 \approx \frac{r - R_{orb}}{c}, \tag{10}$$

where R_{orb} is the mean orbital radius of Earth.

Therefore, an estimate of the magnitude of the amplitude of the annual term is

$$\Delta f \approx f_0 \frac{aR_{orb}}{c^2}. \tag{11}$$

For the case of Pioneer 10 at 40 AU we get

$$\Delta f \approx 14 \text{ mHz}, \tag{12}$$

and at 69 AU

$$\Delta f \approx 4.8 \text{ mHz}, \tag{13}$$

in good agreement with the observed values.

Using data from HORIZONS Web-Interface [14] a more complete analysis of the time variation of Δf has be performed. The residual (that is, simulated Doppler using Vibrating Rays Theory but interpreted under Special Relativity Theory) during 12 years time span is plotted in figure 2. Also the dumped sine best fit of the 50 days average measured by Turyshev et al [18] is plotted showing an excellent agreement between measurements and Vibrating Rays Theory prediction. The negative peaks (i.e., maximum anomalous acceleration) occur during conjunction when the Earth is further apart from the spacecraft, and positive peaks during opposition. Also, the amplitude is larger at the beginning of the plotted interval and decreases with time, as it was observed [4, 18].

5 Flyby anomaly

Like the Pioneer anomaly, the Earth flyby anomaly can be associated to a modeling problem, in the sense that relativistic Doppler includes terms that are absent in the measured signals. The empirical equation of the flyby anomaly is given by Anderson et al [4], which, notably, can be derived using Vibrating Rays Theory, as is done in Part 6 of [13].

Consider the case of NEAR tracked by 3 antennas located in USA, Spain, and Australia (a full description of the tracking system is found in a series of monographs of the Jet Propulsion Laboratory [19]). The receiving antenna was chosen as that having a minimum angle between the spacecraft and the local zenith.

Using available orbital data, a simulated Doppler signal has been calculated using Vibrating Rays Theory. Thus, the simulated residual is obtained by subtracting the theoretical Special Relativity Theory Doppler, from the Vibrating Rays Theory calculation. We observed, however, that the term that contains the velocity of the antennas, that is

$$d = \frac{\gamma_{u_3}}{\gamma_{u_1}} \frac{1 - \hat{\mathrm{r}}_{23} \cdot \mathrm{u}_3/c}{1 - \hat{\mathrm{r}}_{12} \cdot \mathrm{u}_1/c}, \tag{14}$$

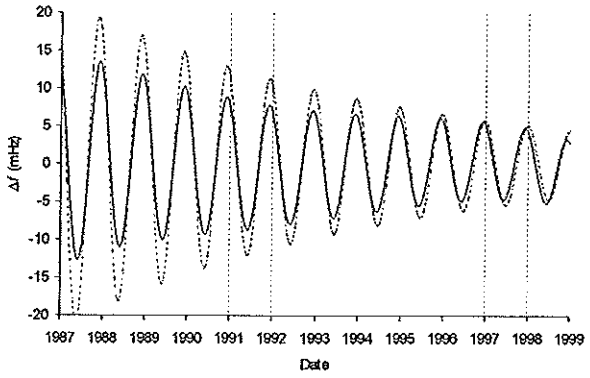

Fig. 2: Annual variation of the frequency difference between Vibrating Rays Theory and Special Relativity Theory (full line) and anomalous dumped sine best fit of the 50 days average measured by Turyshev et al [18] (dashed line), for Pioneer 10 from January 1987 to January 1999.

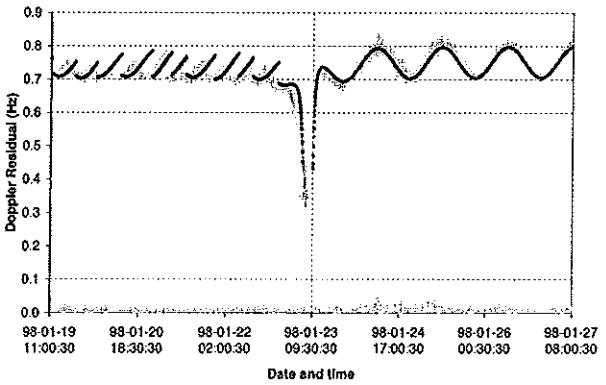

Fig. 3: Fitting the pre- (right half, in red) and post-encounter (left half, in blue) X-band Doppler data residual, for the NEAR flyby under an ideal hyperbolic orbit. Solid lines simulated according to Vibrating Rays Theory. Crosses, actual data extracted from reference [4].

is not enough to completely remove the first order (in u/c) Earth signature (**u** is the velocity of the antenna, 1 refers to the emission epoch and 3 to the reception epoch, as in [13] Part 4).

This is so because the velocity of the antennas is not uniform and the evaluation of the emission time is different for Vibrating Rays Theory and Special Relativity Theory. Then, a small first order term remains. Anyway, since orbital parameters are obtained by periodically fitting the measurements to theoretical orbits, thus a similar procedure is needed for Vibrating Rays Theory. Curiously, by doing so, the first order term is removed. The only difference between orbits adjusted by Special Relativity Theory and Vibrating Rays Theory is a slight rotation of the orbit plane, as mentioned above. Note that in the case of range disagreement (discussed above) two different orbital adjustment would be needed by the Deep Space Network and the Space Surveillance Network due to the different propagation speed. In consequence, it will be impossible to fit a simultaneous measurement, as it seems to happen with the range disagreement.

The final result shows that each antenna produces a sinusoidal residual with a phase shift at the moment of maximum approach. Therefore, if we fit the data with the pre-encounter sinusoid a post-encounter residual remains and vice versa.

In figure 3 are simultaneously plotted the result of fitting the residual by pre-encounter data (right half in red, corresponding to figure 2a of [4]) and by post-encounter data (left half in blue, corresponding to figure 2b of [4]).

Note that the simulated plots are remarkably similar to the reported ones, including the amplitude and phase (i.e., minima and maxima) of the corresponding antenna. The fitting of post-encounter data (blue) can be improved by appropriately setting the exact switching times of the antennas (which are unknown to the author). The flyby Doppler residual exhibits a clean signature of the Vibrating Rays Theory.

6 Conclusions

In this work I have presented observational evidence favoring a dependence of the speed of light on that of the source, in the manner implied in Faraday's ideas of "vibrating rays".

It is remarkable and very suggestive that, as derived from Faraday's thoughts, simply by relating the velocity of light and the corresponding Doppler effect with the velocity of the source at the time of detection, is enough to quantitatively and qualitatively explain a variety of spacecraft anomalies.

Also, it is worth mentioning that a formulation of electromagnetism compatible with Faraday's conception is possible, as shown in [13] Part 8, which is also compatible with the known electromagnetic phenomena. The most remarkable fact of this new formalism is the simultaneous presence of instantaneous (static terms) and delayed (radiative terms) interactions (i.e., local and nonlocal phenomena in the same interaction).

Finally, under Vibrating Rays Theory the manifestation of the movement of the source in the speed of light is more subtle than the naive $c + kv$ hypothesis (k is a constant, $0 \leq k \leq 1$) usually used to test their dependence [8]. Thus, it is also of fundamental importance the fact that, from the experimental point of view, it is very difficult to detect differences between Vibrating Rays Theory and Special Relativity Theory, as discussed in [13], which is also manifest in the smallness of the measured anomalies, and in the non clear manifestation of the effect in usual experiments and observations. For example, it produces a negligible effect on satellite positioning systems, see Part 7 of [13].

I am aware of how counterintuitive these conceptions are to the modern scientist, but also believe that, given the above evidence, a conscientious experimental research is needed to settle the question of the dependence of the speed of light on that of its source as predicted by Vibrating Rays Theory, and

that has been observed during the 1998 NEAR flyby. As a closure, I recall Fox's words regarding the possibility of conducting an experiment on the propagation of light relative to the motion of the source: "*Nevertheless if one balances the overwhelming odds against such an experiment yielding anything new against the overwhelming importance of the point to be tested, he may conclude that the experiment should be performed*" [20].

Acknowledgements

I am thankful to Fernando Minotti who read this paper and improved the manuscript significantly, although he may not agree with all of the interpretations provided in this paper.

Submitted on July 4, 2016 / Accepted on July 8, 2016

References

1. Antreasian P.G., Guinn J. R. Investigations into the unexpected Delta-V increases during the Earth gravity assists of Galileo and NEAR. AIAA Paper No. 98-4287 presented at the AIAA/AAS Astrodynamics Specialist Conference and Exhibit (Boston, August 10-12, 1998).
2. Guruprasad V. Observational evidence for travelling wave modes bearing distance proportional shifts. *EPL*, 2015, v. 110, 54001.
3. Anderson J.D., Laing P.A., Lau E.L., Liu A.S., Nieto M.M., Turyshev S.G. Indication, from Pioneer 10/11, Galileo, and Ulysses Data, of an Apparent Anomalous, Weak, Long-Range Acceleration. *Phys. Rev. Lett.*, 1998, v. 81, 2858–2861.
4. Anderson J.D., Campbell J.K., Ekelund J.E., Ellis J., Jordan J.F. Anomalous Orbital-Energy Changes Observed during Spacecraft Flybys of Earth. *Phys. Rev. Lett.*, 2008, v. 100, 091102.
5. Turyshev S.G., Toth V.T., Kinsella G., Lee S.-C., Lok S.M., Ellis J. Support for the Thermal Origin of the Pioneer Anomaly. *Phys. Rev. Lett*, 2012, v. 108, 241101.
6. de Sitter W. Ein astronomischer Beweis für die Konstanz der Lichgeshwindigkeit. *Z. Phys.*, 1913, v. 14, 429.
7. de Sitter W. Über die Genauigkeit, innerhalb welcher die Unabhängigkeit der Lichtgeschwindigkeit von der Bewegung der Quelle behauptet werden kann. *Z. Phys.*, 1913, v. 14, 1267.
8. Brecher K. Is the Speed of Light Independent of the Velocity of the Source? *Phys. Rev. Lett.*, 1977, v. 39, 1051.
9. Alväger T., Farley F.J.M., Kjellman J., Wallin I. Test of the second postulate of special relativity in the GeV region. *Phys. Lett.*, 1964, v. 12, 260–262.
10. Botermann B., Bing D., Geppert C., et al. Test of Time Dilation Using Stored Li+ Ions as Clocks at Relativistic Speed. *Phys. Rev. Lett.*, 2014, v. 113, 120405.
11. Schrödinger E. Die erfüllbarkeit der relativitätsforderung in der klassischen mechanik. *Ann. der Physik*, 1925, v. 77, 325–336.
12. Faraday M. Thoughts on ray-vibrations. *Phil. Mag. Series 3*, 1846, v. 28, 345.
13. Bilbao L., Bernal L., Minotti F. Vibrating Rays Theory. arXiv: 1407.5001.
14. http://ssd.jpl.nasa.gov
15. Markwardt C.B. Independent Confirmation of the Pioneer 10 Anomalous Acceleration. arXiv: gr-qc/0208046.
16. Anderson J.D., Laing P.A., Lau E.L., Liu A.S., Nieto M.M., Turyshev S.G. Study of the anomalous acceleration of Pioneer 10 and 11. *Phys. Rev. D*, 2002, v. 65, 082004.
17. Levy A., Christophe B., Reynaud S., Courty J-M., Brio P., Mtris G. Pioneer 10 data analysis: investigation on periodic anomalies. Journées scientifiques de la SF2A, Paris, France, 2008, 133–136 (hal-00417743).
18. Turyshev S.G., Anderson J.D., Laing P.A., Lau E.L., Liu A.S., Nieto M.M. The Apparent Anomalous, Weak, Long-Range Acceleration of Pioneer 10 and 11. arXiv: gr-qc/9903024.
19. DESCANSOTeam, Jet Propulsion Laboratory, California Institute of Technology. http://descanso.jpl.nasa.gov/Monograph/mono.cfm (accessed July 2014).
20. Fox J.G. Experimental Evidence for the Second Postulate of Special Relativity. *Am. J. Phys.*, 1962, v. 30, 297.

Editorial Comment

This paper plays an importance in the understanding of the physical observable velocity of light that differs from the world-invariant in the General Theory of Relativity.

Defining physical observable quantities in the General Theory of Relativity is not a trivial problem. This is because we are looking at objects in a four-dimensional space-time, and we have to determine which components of these four-dimensional tensor quantities are physically observable. A complete mathematical theory for calculating physically observable quantities in the four-dimensional space (space-time) of General Relativity was introduced in 1944 by Abraham Zelmanov, and is known as the *theory of chronometric invariants*[*]. Landau and Lifshitz in §84 of their *The Classical Theory of Fields* also introduced physically observable time and observable three-dimensional intervals similar to Zelmanov. But they limited themselves only to this particular case, while only Zelmanov arrived at the versatile mathematical theory. A compendium of Zelmanov's theory of physical observable quantities can also be found in the books[†].

In short, physically observable are the projections of four-dimensional quantities onto the time line and the three-dimensional spatial section of the observer, which can be non-uniform, deformed, curved and rotating. These projections are calculated through the special projecting operators which take all the aforementioned factors into account. In particular, the physical observable velocity of light differs from the world-invariant, and is depended on the gravitational potential and the rotation velocity of the observer's space. In ultimate physical conditions, as is shown in Chapter 5 of *Particles Here and Beyond the Mirror*[†], the observable velocity of light can even become zero, that is verified by the frozen light experiment (Lene Hau, 2001).

Even more. In a physical space (space-time metric) wherein is a shift at one of the spatial directions (that means a spatial anisotropy), the observable velocity of light is depended on the signal source's velocity at this preferred direction. We drafted such a space-time metric in the last decade.

Einstein's postulates have now only a historical meaning. Once Einstein moved his theory on the mathematical basis of Riemannian geometry, he found that all the postulates are the manifestations of geometry of Riemannian spaces. It is as well true about the world-invariant of the velocity of light. In a space, which is free of gravitation, is uniform, non-deformed, and non-rotating, the physical observable velocity of light coincides with the world-invariant. However in a real physical space it does not.

For this reason the experimental compendium and the analysis presented in Bilbao's paper will maybe give a new fresh stream in search for the further theoretical predictions of the General Theory of Relativity.

Dmitri Rabounski, Editor-in-Chief
Larissa Borissova, Assoc. Editor

[*]Zelmanov A. Chronometric invariants. American Research Press, Rehoboth (NM), 2006. Zelmanov A. Chronometric invariants and accompanying frames of reference in the General Theory of Relativity. *Soviet Physics Doklady*, 1956, v. 1, 227–230.

[†]Borissova L. and Rabounski D. Fields, Vacuum, and the Mirror Universe. 2nd ed., Svenska fysikarkivet, Stockholm, 2009. Rabounski D. and Borissova L. Particles Here and Beyond the Mirror. 3rd ed., American Research Press, Rehoboth (NM), 2012.

A Letters Journal Exploring the Frontiers of Physics

September 2016

EPL, 115 (2016) 54004
doi: 10.1209/0295-5075/115/54004

www.epljournal.org

Comment

Comment on "Observational evidence for travelling wave modes bearing distance proportional shifts" by V. Guruprasad

Luis Bilbao[a]

Universidad de Buenos Aires, Consejo Nacional de Investigaciones Científicas y Técnicas, Instituto de Física del Plasma (INFIP), Facultad de Ciencias Exactas y Naturales - Buenos Aires, Argentina

received 7 July 2016; accepted in final form 13 September 2016
published online 11 October 2016

PACS 41.20.Jb – Electromagnetic wave propagation; radiowave propagation
PACS 84.40.Ua – Telecommunications: signal transmission and processing; communication satellites
PACS 02.30.-f – Function theory, analysis

In a recent paper, Guruprasad [1] proposed an explanation of spacecraft flyby anomalies based on a theoretical model of traveling waves.

In order to contrast the theory against measurements, experimental data from the measured range disagreement of 1998 NEAR flyby were used [2]. (I believe that "disagreement" is a better term than "error" to describe this anomaly of the NEAR spacecraft.) Although the disagreement was detected during an Earth flyby, it should be distinguished from the so-called flyby anomaly [3] which refers to an unexpected energy increase during Earth flybys of spacecraft.

The ranging data are obtained from the time delay of the radio signals, and are independent of the Doppler data, although the time-integrated Doppler frequency should equal the range variation. The range disagreement detected by Antreasian and Guinn [2] is the difference in the range measured by the Millstone and Altair tracking stations of the Space Surveillance Network (SSN) relative to the expected range according to the trajectory obtained from the Deep Space Network (DSN). The actual flyby anomaly [3] remains unexplained in Guruprasad's paper.

The main objections to the paper by Gurusprasad, besides the former one, are the following: a) loose estimates of orbital data are used, while the orbital parameters are readily available [2]; b) an unrealistic relationship between range error and range is used; and c) no statistical significance of the agreement between model and measurements is given.

An example of the poor estimates is given on page 5, left column, where it is written "The uniformity of the 10 min ticks in the equatorial view ([9], fig. 1 and of similar ticks in the north polar view ([14], fig. 9), which are expanded due to projection, suggest that the mean speed $v_o \equiv 6.85\,\mathrm{km\,s^{-1}}$ would be adequate for present purposes." In other words, the used mean radial speed is obtained from the author's interpretation of a published figure, instead of actual data. In fig. 1 total and radial speeds of NEAR are plotted. The mean radial velocity is about 8 km/s during SSN traking, that is, 17% larger than the used estimate.

The consequence is that the fit of fig. 1 of [1] changes appreciably. The fit relies on a relationship described on page 2, right column, as "Denoting the instantaneous range errors as Δr, and the radial speed as v_o, the lag times in the figure are given by $\Delta t = \Delta r/v_o$, and the one-way ranges, by $r = c\Delta t - r_e \approx c\Delta r/v_o - r_e$, where $r_e \equiv 6.371\,\mathrm{km}$, the Earth's radius." That is, a linear relatioship between range, r, and range disagreement, Δr, is proposed. In fig. 2, the plot of the above relationship using both $v_o = 6.85\,\mathrm{km/s}$ (the asymptotic speed used by Gurusprasad), and $v_o = 8\,\mathrm{km/s}$ (the actual speed) is given. Also, they are compared to the actual relationship for Millstone (Δr from measurements and r from orbital data). Differences are so large (as much as more than half the Earth radius) that clearly invalidate the relationship with the radial speed proposed by Gurusprasad.

Further, although the above relationship can be presented as a *de facto* correlation, from a physical viewpoint there is no justification on why range (r) and Earth radius (r_e) may appear arithmetically added. The Earth

[a]Present address: INEI, Universidad de Castilla-La Mancha - Ciudad Real, Spain; e-mail: bilbao@df.uba.ar

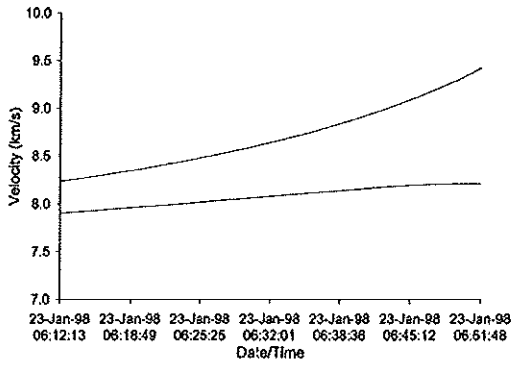

Fig. 1: (Colour online) Speed of NEAR (green, upper line) and radial speed (magenta, lower line) during SSN tracking.

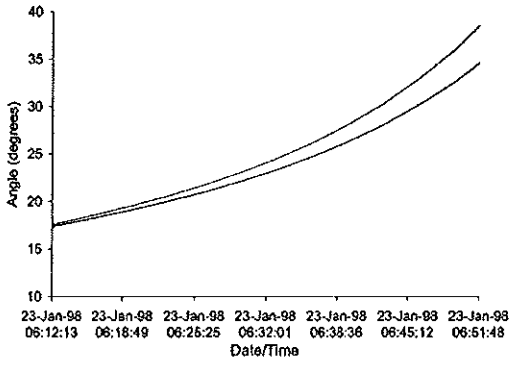

Fig. 3: (Colour online) Angle between trajectory of NEAR and line of sight to SSN antennas: Millstone (blue, lower line) and Altair (red, upper line).

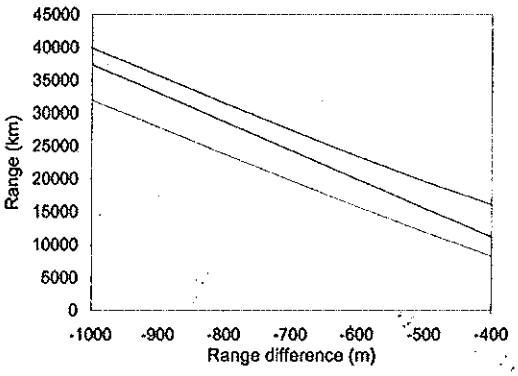

Fig. 2: (Colour online) Range as a function of range difference. Guruprasad's proposed model with $v_o = 6.85\,\mathrm{km/s}$ [1] (magenta, middle line), proposed model with $v_o = 8\,\mathrm{km/s}$ (the actual speed) (orange, lower line), and actual relationship for Millstone (green, upper line).

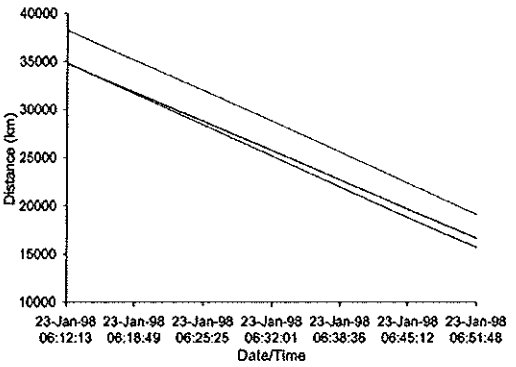

Fig. 4: (Colour online) Orbital radius of NEAR (green, upper line), range from Millstone (blue, middle line) and range from Altair (red, lower line).

radius relates to the position of the detectors, but the direction from the Earth center to the radar is not parallel to the range, which points from the radar to the spacecraft. Thus, one should expect the appearance of an angle cosine in the formula.

Another example of poor (wrong) estimates is on page 5, right column, where it is written "the trajectory pointed towards Millstone initially, implying a faster initial decrease of the range,...". This is not true. In fig. 3 the angle between the trajectory and the line of sight to the SSN antennas are plotted. As can be seen, initially the trajectory points equally to both antennas (about 17.5 degrees). Further, as is shown in fig. 4, initially (and during the whole coverage) Altair has a faster decrease of the range, not Millstone as stated by Guruprasad.

Finally, no statistical significance is referred to in the paper. Only vague percentage figures are mentioned. For example, referring to the one-way delay on page 5, left column, it is said to be "about 25% smaller than in fig. 1." Or, the Doppler amplitude, "These are about 20% of the reported $760\,\mathrm{mHz} = 13.5\,\mathrm{mm\,s^{-1}}$." How good are these figures? Do they have any statistical significance?

Orbital parameters are readily accesible, thus the actual orbit of spacecrafts is easily obtained. A test of the theory could be conducted in a more precise way.

As presented by Guruprasad, the theory seems to roughly agree with wrong estimates, thus giving the impression that the theory is not supported by actual data.

REFERENCES

[1] Guruprasad V., *EPL*, **110** (2015) 54001.
[2] Antreasian P. G. and Guinn J. R., *Investigations into the unexpected Delta-V increases during the Earth gravity assists of Galileo and NEAR* (AIAA) 1998, paper No. 98–4287.
[3] Anderson J. D., Campbell J. K., Ekelund J. E., Ellis J. and Jordan J. F., *Phys. Rev. Lett.*, **100** (2008) 091102.

EXACTAS UBA

Ref.: Exp. (FCEN) Nº 475.554/03

Ciudad de Buenos Aires, 27 MAR 2017

VISTO lo dispuesto en el artículo 50º del Estatuto Universitario que instituye el Año Sabático para profesores regulares de la Universidad,

CONSIDERANDO:

Que por Resolución CD Nº 2189/15 se solicitó al Consejo Superior se autorice al Dr. Luis Ernesto Bilbao Profesor Regular Adjunto con dedicación exclusiva del Departamento de Física a hacer uso del Año Sabático,

Que por Resolución CS Nº 3665/15 se aprobó dicha solicitud otorgando licencia desde el 1 de febrero de 2016 hasta el 31 de enero de 2017,

Que en cumplimiento con el Art. 12º de la Resolución CS Nº 4518/93, el Dr. Luis Ernesto Bilbao presentó su informe de actividades,

Que es necesario cumplir con lo establecido por los Art. 13º y 14º de la citada resolución,

Lo aconsejado por la Comisión de Enseñanza, Programas y Planes de Estudio,

Lo actuado por este cuerpo en la sesión realizada en el día de la fecha,

En uso de las atribuciones que le confiere el art. 113º del Estatuto Universitario,

EL CONSEJO DIRECTIVO DE LA FACULTAD DE CIENCIAS EXACTAS Y NATURALES
RESUELVE:

Artículo 1º: Aprobar el informe correspondiente a las actividades desempeñadas por el Dr. Luis Ernesto Bilbao durante su Año Sabático.

Artículo 2º: : Enviar un ejemplar del informe a la Biblioteca de esta Facultad.

Artículo 3º: Regístrese, notifíquese a quienes corresponda, elévese al Consejo Superior y cumplido, archívese.

RESOLUCIÓN CD Nº 0460

Dr. JORGE ZILBER
SECRETARIO ACADEMICO ADJUNTO

Dr. JUAN CARLOS REBOREDA
DECANO